

**KERNFORSCHUNGSZENTRUM
KARLSRUHE**

Oktober 1969

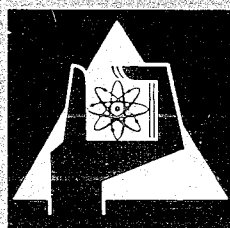
KFK 1022
EUR 4303 e

Institut für Angewandte Reaktorphysik
Institut für Neutronenphysik und Reaktortechnik

SNEAK-4

A Series of Physics Experiments for KNK-II

Compiled by
P. Engelmann



GESELLSCHAFT FÜR KERNFORSCHUNG M. B. H.

KARLSRUHE

Oktober 1969

KFK 1o22
EUR 43o3 e

Institut für Angewandte Reaktorphysik
Institut für Neutronenphysik und Reaktortechnik

SNEAK-4

A Series of Physics Experiments for KNK-II¹

Compiled by
P. Engelmann

With contributions from

L. Barleon, W. Bickel, H. Bluhm, R. Böhme, K. Böhnel, D. Eitner², P. Engelmann,
G. Fieg, E.A. Fischer, G. Günther, M. Müller, W.J. Oosterkamp, A.M. Raberain³,
E. Ruppert², W. Seifritz, P.L. van Velze³, H. Werle, H. Wilhelm², G. Wittek, and
J. Woite

Gesellschaft für Kernforschung mbH., Karlsruhe

¹Work performed within the association in the field of fast reactors between the European Atomic Energy Community and Gesellschaft für Kernforschung mbH., Karlsruhe

²INTERATOM, Bensberg

³EURATOM

Table of Contents

	<u>Page</u>
1. Introduction (P. Engelmann)	3
2. Methods of Calculation (A.M. Raberain, D. Eitner, H. Wilhelm)	5
3. Reactivity Determinations (W. Bickel, E. Ruppert, G. Wittek)	9
4. Reaction Rates (J. Woite, R. Böhme, E.A. Fischer, P.L. van Velze)	12
5. Doppler Effect (L. Barleon, E.A. Fischer, W.J. Oosterkamp)	18
6. Neutron Spectrum (M. Müller, G. Fieg, H. Werle, H. Bluhm)	20
7. Material Worth Measurements (G. Günther, E.A. Fischer)	23
8. Prompt Neutron Decay Constant (K. Böhnel, W. Seifritz)	25
9. Sodium Worth Studies (W. Bickel, P. Engelmann)	28
10. Use of SNEAK-4 Results for the KNK-II Design (D. Eitner, P. Engelmann, E. Ruppert)	29

ABSTRACT

At the end of 1968 a three months program of neutron physics experiments was performed at SNEAK for the investigation of some nuclear properties of the KNK-II reactor. The experiments were conducted by the Karlsruhe Nuclear Research Centre in close cooperation with INTERATOM. The results of the measurements on SNEAK assemblies 4A and 4B are reported and compared with calculations. The experimental results of critical mass and reactivities, control rod worths, Doppler coefficient, and power distribution were used to draw conclusions for the KNK-II design.

KURZFASSUNG

Im Herbst 1968 wurden in der SNEAK neutronenphysikalische Experimente zur Untersuchung der nuklearen Eigenschaften des KNK-II Reaktors durchgeführt. Das dreimonatige Versuchsprogramm wurde vom Kernforschungszentrum Karlsruhe in enger Zusammenarbeit mit INTERATOM geplant und durchgeführt. In diesem Bericht werden die Ergebnisse der Messungen an den SNEAK-Anordnungen 4A und 4B zusammengefaßt und mit Rechnungen verglichen. Aus dem Vergleich der experimentellen Ergebnisse für kritische Masse, Reaktivitätswerte, Steuerstabwerte, Dopplerkoeffizient und Leistungsverteilung mit Rechnungen werden Schlüsse für die Auslegung des KNK-II gezogen.

1. INTRODUCTION

At Karlsruhe the sodium-cooled experimental reactor KNK designed by INTERATOM will become operational in 1969. After successful operation of the first thermal zirconium hydride moderated core KNK-I the insertion of a second core, KNK-II, with a fast neutron spectrum is planned. The reactor KNK-II will be the first experimental fast power reactor in Germany. Its main purpose is to serve as a test facility for fast breeder fuel elements. The requirement of a high rating in the test pins and a negative power coefficient of the core lead to a KNK-II design with two core zones (ref. 1): the inner zone serving as the actual test bed will be fueled with PuO_2UO_2 pins with about 30 w/o PuO_2 , the UO_2 of the fuel will be highly enriched in ^{235}U in order to obtain a high linear rod power of about 450 W/cm. The surrounding driver zone which makes the core critical will have UO_2 fuel with an enrichment of about 35%. The neutron spectrum of the driver will be slightly moderated by means of steel canned zirconium hydride pins. The driver thus will contribute a large negative Doppler coefficient providing for an overall negative power coefficient of KNK-II. The volume of the test zone will be 60 l, that of the driver 240 l. The core will be surrounded by a sodium-cooled SS reflector. Eight B_4C control rods are foreseen in the driver at the KNK-I control rod positions. The calculation of this small and very heterogeneous reflected two-zone core is rather difficult. It was therefore felt necessary to check the calculational methods and cross section data by experiments in the fast zero power reactor SNEAK.

A period of three months was available for the experiments in SNEAK. The program was set up in discussions between GfK and INTERATOM in order to obtain a maximum of information within this short time interval.

The experiments were made in three major steps:

- 1) a clean reflected two-zone core SNEAK-4A was assembled consisting of test-zone, driver-zone, and reflector;
- 2) into this core 8 sodium followers were introduced at the KNK-II control rod positions (SNEAK-4B-1);
- 3) the sodium followers were partly replaced by B_4C absorber rods (SNEAK-4B-2 and 4B-3).

The main purpose of the first two steps was to check the data sets and calculational methods used on systems which were similar to KNK-II but of a simpler geometry. The last step was devoted to control rod studies. In assembly 4B-2 six sodium followers of the inner ring were replaced by half

inserted B_4C absorber rods. This configuration was closest to the real KNK-II core at start-up while SNEAK-4B-1 is close to the KNK-II core at the end of the fuel life time. In assembly 4B-3 3 sodium followers were replaced by fully inserted B_4C rods.

The core geometry of KNK-II could be mocked-up rather well in spite of the fact, that the hexagonal fuel subassemblies had to be approximated by the square lattice of SNEAK. Each KNK-II control rod was replaced by 4 SNEAK elements. The centre of the core was shifted towards the south east of the matrix in order to have pile oscillator positions available in both test and driver zones (ref. 2). Outside the steel reflector a blanket of depleted uranium metal from the previous core was left in place in order to save time in reloading. The influence of the non-symmetric shape of the blanket was calculated to be $<6 \cdot 10^{-4}$ in k.

Some limitations arose in the simulation of the material composition. The driver composition which was kept the same in all three experiments could be closely approximated, the test zones, however, always contained too much ^{238}U because most of the SNEAK plutonium is fabricated into UO_2PuO_2 plates with only 25% PuO_2 content. A close simulation, therefore, was possible only in 4 SNEAK elements where pure PuO_2 plates could be used.

A comparison of the material compositions in KNK-II and SNEAK is given in Table 1. The composition of the test zone was varied from step to step in order to keep the assembly critical in the given geometry. Reflector, blanket, sodium followers, and control rods could be simulated satisfactorily.

In SNEAK-4A the following quantities were measured:

critical mass,
neutron spectrum in test zone and driver from several eV up to 6 MeV,
radial reaction rate distributions,
reactivity worths of selected materials,
the $\beta/1$ ratio,
Doppler effect in the driver,
effect of hydrogen arrangement on reactivity and Doppler effect.

In SNEAK-4B the main interest rested on measurements of the Doppler effect in the environment of sodium followers and B_4C absorber rods, the coarse and fine distribution of reaction rates near control rods and zone boundaries, the control rod worth, and the critical masses in the various configurations.

2. METHODS OF CALCULATION

2.1 Codes Used in the Calculations

2.11 Diffusion calculations

The basic assemblies referred to as 4A, 4B-1, 4B-2, and 4B-3 as well as a few intermediate configurations in the course of loading the control rods were calculated by the Nuclear Research Centre of Karlsruhe and by INTERATOM at Bensberg (Köln), using in both places the calculational methods and nuclear codes which were thought to be best suited for handling such an intricate core.

None of the configurations could be properly calculated by one-dimensional codes. All the k_{eff} calculations were therefore carried out either with the two-dimensional diffusion codes DIXY of the Karlsruhe nuclear code system NUSYS and MUGDI of INTERATOM or with the three-dimensional Monte Carlo Code MOCA (ref. 3) available at INTERATOM.

In order to check a computational model applied by INTERATOM for the KNK-II project lay-out additional calculations were done for the assemblies SNEAK-4B-1 and 4B-2 (with sodium followers and with boron carbide control rods) using the cell method. In this method for the diffusion calculations the Na-followers and the B_4C rods were homogenized with the neighbouring elements of the test and driver zone, instead of considering them as a separate mixture arranged in a ring with a volume equal to that of the simulated rods. The effect of the detailed structure within such an homogenized region was determined by a cell calculation. A cell was assumed to consist of one control rod or Na-follower (=4 SNEAK elements) surrounded by 12 core elements. It was computed with a S_n program using appropriate boundary conditions and axial bucklings, and then homogenized according to the calculated flux weights.

One-dimensional codes were used for the determination of secondary parameters such as heterogeneity corrections, worth of central elements, or for comparative calculations with different cross section sets.

However, the effective delayed neutron fraction β_{eff} was also calculated in one-dimensional cylindrical geometry because a suitable two-dimensional program was not yet available. This is not completely satisfactory because the result might be affected by the presence of the axial blanket and should therefore be given a two-dimensional treatment. A rough estimate shows that the uncertainty of β_{eff} due to the one-dimensional treatment is only in the order of 1%.

2.12 S_n-correction

Two-dimensional S_n calculations had to be simulated by one-dimensional codes: the S_n calculations were carried out successively in the radial direction in cylindrical geometry, and axially in slab geometry for each of the two radial zones of the core. The total correction factor is finally obtained by comparison with identical diffusion calculations, appropriate weighting of the radial zones and simple adding of the axial and radial correction factors. When applying the cell method a total S_n correction was derived from one-dimensional axial and radial S_n calculations for the core together with the cell results.

Both methods agree rather well and the discrepancy between the respective results for the S_n correction lies between 3% and 5% in k, the total S_n correction being of the order of 2%. In the S_n calculations the order n=4 proved to be sufficient for satisfactory results.

2.13 Heterogeneity corrections

In spite of the cell structure of the SNEAK cores all the calculations were first carried out for homogenized mixtures; the actual heterogeneous structure of the assemblies was taken into account in the form of a correction factor obtained by one-dimensional perturbation calculations with "heterogeneity corrected" cross sections as supplied by the multigroup cell program ZERA (ref. 4).

2.14 Streaming effects

The axial leakage in the sodium followers, which is given approximately by

$$\int_{\text{Na-Zones}} DB_{\text{ax}}^2,$$

accounts for about 5% in k. However, for dilute materials such as sodium and in particular for a geometry where the mean free path in the core mixture is of the same order of magnitude as the thickness of the sodium zone, diffusion theory considerably overestimates the leakage. From considerations similar to those given by Bonalumi (ref. 5) it can be shown that a correction of the order of $B_{\text{ax}}^2 \cdot \lambda_{\text{tr Na}}^2$ must be applied to the calculated leakage, resulting in an increase of about 0.5% in k_{eff}.

2.2 Group Structure and Cross Section Sets

2.21 Group structure

All the calculations made at Karlsruhe as well as the Monte Carlo calculations of INTERATOM were carried out with 26 energy groups. The group structure is that of the Russian ABN set (ref. 6). Most k_{eff} calculations were also performed with 4 energy groups, using volume-averaged condensation spectra found for the different zones by one-dimensional calculations. The group structure for both 26 and 4 group sets is shown in Table 2. The discrepancy between the results of 4 group and 26 group calculations is lower than 0.5%. It lies therefore within the precision margin to be expected from the calculation of an assembly which would in fact require a three-dimensional treatment.

2.22 Cross section sets used

The calculations were carried out using the 26 group KFK-NAP-PMB set (ref. 7). This set is very similar to the SNEAK set which was prepared for the calculations of steam-cooled reactors (ref. 7,8). The differences are: 1) the scattering matrix was recalculated on the basis of a sodium-cooled breeder spectrum and 2) the capture and fission cross sections of uranium were modified according to measurements by Pönitz and Menlove and recommendations of Beckurts (ref. 9).

Comparative calculations were carried out with other cross section sets, particularly with the ABN set and with newly developed sets referred to as PUO2RE and MOXTOT set respectively (ref. 10). These sets use the same weighting spectrum as the SNEAK set but contain the following modifications: PUO2RE uses improved values of the capture/fission ratio of plutonium according to Gwin and improved data for the higher plutonium isotopes; MOXTOT in addition uses ^{238}U capture data of Moxon in the range of 500 eV to 100 keV.

2.3 Geometrical Models

With the exception of assembly 4B-2 the k_{eff} calculations were carried out in X-Y geometry which allows a precise description of the various radial zones and a good simulation of the changes made in the assemblies by the loading of control rods or differently enriched fuel elements. In order to keep the number of mesh-points within a reasonable limit only half-cores could be considered. Therefore assemblies with an odd number of control rods of a

given type (sodium or B_4C) had to be calculated in two steps representative of the two core halves with different numbers of rods. The leakage in axial direction was simulated by energy- and zone-dependent transverse bucklings obtained by two-dimensional calculations in R-Z geometry. This introduces an error of the order of 0.15% in k_{eff} . The difficulty in the determination of the axial bucklings was the main obstacle to the use of the two-dimensional X-Y code.

The Monte Carlo code is able to simulate the complete (zone-wise homogenized) three-dimensional structure of the cores but the results are affected by a statistical error which within realizable running-times (80 generations of a population of 90 neutrons were followed) amounts to about 0.5% in k_{eff} , and is, consequently, not suited for the calculations of small reactivity changes.

2.4 Calculation of Reaction Rates

The reaction rate distributions were calculated with the two-dimensional diffusion code DIXY in 26 energy groups. A number of these calculations were also run with 4 energy groups. The small discrepancy between both results is probably due to the use of condensation spectra averaged over entire zones for the 4 group calculations.

The reaction rates were generally calculated in X-Y geometry allowing a precise representation of the various core configurations. For assembly 4B-2 which contains half inserted control rods X-Y calculations were performed for the upper and lower part of the core. In addition a R-Z calculation was made providing an estimate of the respective values of the reaction rates at these two levels.

For the calculation of reaction rates in regions not containing the isotope under consideration (e.g. Pu reaction rates in the steel reflector or the driver zone) these were added in very small quantities (10^{13} at/cm³) to the actual composition introducing thereby a negligible error in the self-shielding factor of the core materials. The self-shielding of the added isotopes corresponds to infinite dilution because of the very low density.

Another source of error lies in the fact that for reducing the number of mesh-points the cores were very often made symmetrical bringing about a certain distortion in the statistical weight of the different regions.

These errors, however, have been reduced to a minimum and no corrections for them were made in the calculations.

3. REACTIVITY DETERMINATIONS

3.1 Experimental Method

Reactivities and changes of reactivity connected with loading changes in the core were measured using calibrated shim rods. The change of reactivity is equal to the difference of the excess reactivity in the shim rods before and after the loading change.

Because of the neutrons generated by spontaneous fission of plutonium and (α, n) effects in the oxygen reactivities were compared at a fixed power level corresponding to a slightly subcritical state (about 2 ϵ subcritical).

The relative uncertainty in the measured reactivity worths is up to 10%. This error is mainly due to uncertainties in the calibration of the shim rods and to the fact, that the rods were not recalibrated after each loading change so that interpolations had to be made. The 10% also include the error in β_{eff} .

The SNEAK shim rods were calibrated by driving them stepwise into or out of the core. The procedure started from a constant neutron flux level. The flux was measured with three BF_3 ionization chambers located outside the radial reactor blanket. Chamber current and rod position were recorded simultaneously on punched paper tape. From this record the reactivity characteristic of the rod was calculated by solving the inverse kinetics equations on the DDP 124 computer. The uncertainty in the calibration due to deviations from point reactor kinetics could be estimated from the difference of the results obtained from the three chambers, which had an azimuthal distance of about 120 degrees from each other.

3.2 Basic Assemblies Investigated

Four configurations, SNEAK-4A, SNEAK-4B-1, SNEAK-4B-2, and SNEAK-4B-3 were investigated (Figs. 1 and 2). The composition of these assemblies is given in Figs. 1, 2, 3, and 4 and Tables 1 and 4. Measured and calculated k_{eff} values are compared in Table 5.

3.3 Changes Within the Basic Assemblies

3.31 Changes of enrichment of fissile material

In the test zone the reactivity effect of inserting a fuel element with different enrichment was measured. For example in SNEAK-4B-1 an element of type 14 was replaced by an element of lower enrichment (type 13) and by an element of higher enrichment (type 16). The results of these measurements are listed in Table 6.

3.32 Simulation of KNK-II control rods

The stepwise insertion of KNK-II control rods was simulated in going from SNEAK-4B-1 to 4B-3. Four SNEAK elements filled with B_4C powder in SS boxes (type 19) represented one KNK-II control rod. The resulting reactivity losses were compensated by a stepwise increase of the fuel enrichment in the test zone. Some results of the control rod experiments are given in Table 7, the core configurations are shown in Figs. 1 and 2.

3.33 SNEAK elements with KNK-II composition

In the centre of the test zone of SNEAK-4B-1 a KNK fuel element was simulated by 4 SNEAK elements with a composition similar to that of a true KNK fuel element (type 24). These elements are designated as "SNEAK elements with KNK-II composition".

The reactivity increase caused by inserting these highly enriched elements was compensated by stepwise removing fuel elements at the driver reflector interface. The results of this measurement are compared with calculation in Table 8.

~~3.34 Simulation of a radial breeder blanket~~

In a small sector of SNEAK-4B-2 (see Fig. 2) reflector elements filled with steel (type 11) or depleted uranium (type 3) were replaced by elements filled with natural uranium and sodium (type 20). The resulting change in reactivity is listed in Table 9. No calculation was made in this case because of the complex geometry.

3.4 Discussion of the Results

The k_{eff} values of the assemblies SNEAK-4A, 4B-1, and 4B-2 are underestimated by about 1.5% (see Table 5). Diffusion and transport calculations are in excellent agreement with results found by the Monte Carlo method.

However, for assembly 4B-3 with 5 sodium followers and 3 fully inserted control rods the agreement is not so good. The ratio of calculated to measured k_{eff} values is 0.990 and 0.994 using analytical (diffusion and transport) and Monte Carlo methods, respectively.

The reactivity changes in going from assembly 4A to 4B-1 and from 4B-1 to 4B-2, respectively, are well predicted by calculations. The same agreement between experiment and calculation is found in the intermediate steps 4B-1 to 4B-1-1 and 4B-1-2 (Table 7). In these experiments in each step absorber material was brought into the reactor and the fuel enrichment in

the test zone was increased at the same time. The effect of increasing the fuel enrichment is well predicted by diffusion calculation (see Table 6). It might therefore be concluded that the reactivity worth of a single fully inserted control rod (4B-1-1) as well as that of a ring of partly inserted control rods (4B-2) can be satisfactorily calculated.

For the transition from SNEAK-4B-1 to 4B-3, however, a somewhat larger deviation between experimental and calculated reactivity change is realized (Table 5). The k_{eff} value of assembly 4B-3 calculated by diffusion theory was obtained as the average of calculations for 4 and 2 control rods, respectively. It seems that this simplification does not quite represent the actual behaviour. The calculated reactivity difference 4B-1 to 4B-3 is $\Delta k_{eff} = 0.9\%$, while the experimental result is 0.53%. Looking at these discrepancies, however, one must keep in mind that the reactivity worth of the three fully inserted control rods is $\Delta k = 7.2\%$; the relative error in the calculation of the control rod worth is thus only about 5%.

The effect of replacing 4 central SNEAK elements by those with KNK-II composition is underestimated by 15% with the NAP-PMB set as shown in Table 8. This may be due to the uncorrect multigroup data for Pu240 in the cross section set.

The comparative 1-dimensional diffusion calculations with other multigroup sets yielded the following reactivity changes as compared to the NAP-PMB set ($k_{eff,x} - k_{eff,NAP-PMB}$):

	<u>SNEAK-PMB</u>	<u>ABN</u>	<u>PUO2RE</u>	<u>MOXTOT</u>
4A	-0.15%	+2.1%	+0.43%	+1.16%
4B-1	-0.15%	+2.4%	+0.60%	+1.29%

The SNEAK-PMB values are slightly worse than the NAP-PMB data while the PUO2RE set and especially the MOXTOT set give significant improvements in the prediction of k_{eff} . The good prediction with the MOXTOT set is probably due to the fact that the effects of overreactive ^{235}U data and underreactive ^{239}Pu data in this two-zone core just about cancel. The ABN set overestimates reactivity by about 1%, as has been observed in other assemblies before.

4. REACTION RATES

Reaction rates were determined in SNEAK-4A and in various configurations of SNEAK-4B as a function of position with fission and BF_3 chambers and by foil or plate activation. Main purpose of the experiments was to find out the accuracy with which the spatial rate distribution and thus the power profile can be predicted in these complex core configurations.

4.1 Experimental Technique

4.1.1 Chamber measurements

The radial reaction rate distributions at core midplane were measured in the horizontal channel ($Y=19$) using small cylindrical fission chambers (^{235}U , ^{238}U , ^{239}Pu) of the 20th Century Electronics type FC4. In addition to the main isotope the chamber deposits contained the following impurities:

^{235}U chamber : ^{234}U 1.2% ; ^{236}U 0.27% ; ^{238}U 5.4%
 ^{238}U chamber : ^{234}U 0.005% ; ^{236}U 0.005% ; ^{235}U 0.3%
 ^{239}Pu chamber : ^{240}Pu 1.0% .

The active length of the chambers is 2.5 cm. Measurements were also made with a ^{10}B counter (Wood MN-1) which had about the same dimensions as the fission chambers.

The statistical error of the measurements was always smaller than 1%. The environment of the chambers, however, is slightly perturbed by the channel arrangements (see Fig. 5). This means, that the results of the traverse measurements are not quite representative of the rates in the unperturbed case, especially near boundaries. Furthermore, the steel guiding tube (Fig. 5) is empty outside the length of the chamber, so that neutron streaming occurs along the axis of the channel. This effect perturbs mainly the ^{10}B measurements.

4.1.2 Foil measurements

Fission rates of ^{235}U , ^{238}U , and ^{239}Pu as well as the capture rate of ^{238}U were determined by foil activation.

For the uranium measurements pairs of foils of depleted (0.4 w/o ^{235}U) and enriched (20.04 w/o ^{235}U) uranium were irradiated. The 0.1 mm thick foils were 9.5 mm in diameter for the radial and 25.4 mm in diameter for the axial traverses. The ^{238}U capture rate was determined using the method described in ref. 11 while the fission rates were determined by counting the fission product γ -activity above 660 keV (ref. 12). The foils were repetitively counted in a forward and reverse cycle in order to eliminate problems arising from the complex decay law of the fission products.

The uranium foils were irradiated at various positions within the unit cell in both test and driver zone to determine the fine structure of the rate distributions and to obtain cell averaged reaction rates for comparison with the calculated rate distributions.

In the hard spectrum test zone no pronounced fine structure of the fission and capture rates within the unit cell was found: the deviations hardly exceeded the experimental uncertainty of $\pm 2\%$. The much larger fine structure in the soft spectrum driver zone as measured in position 16/20 is shown in Fig. 6.

Also shown are the average reaction rates of the platelets as calculated with the ZERA code. However, as the foils were positioned between the platelets, one can only make a qualitative comparison between theory and experiment. The results are satisfactory, except for the fission rate in ^{238}U , where the fine structure is underpredicted. This rate, however, contributes only little to the power distribution, as is made obvious by the scale on the right side of Fig. 6.

Plutonium fission rates were measured by irradiating 0.3 mm thick, 14 mm diameter foils of a 6 w/o Pu-Al alloy inside an Al plate of the unit cell. The γ -activity of the irradiated foils was measured in the range 0.55 to 1.1 MeV and above 1.1 MeV. In addition to the foil activity the γ -activity of normal PuO_2UO_2 platelets was measured before and after a 200 Wh operation period. In this case, the low energy γ -radiation was removed using a 4 mm Pb shield and collimators. The fission rate was determined from the γ -activity above 1.3 and 2.5 MeV, respectively.

4.2 Method of Calculations

The methods of calculation were described in chapter 2.4. Most calculations were made in 2-dimensional diffusion theory for homogenized core regions using the 26 group NAP-PMB cross section set. However, the radial fission rate traverses in core 4A were also calculated with cross sections which are flux-averaged over the heterogeneous cell. These cross sections were obtained with the ZERA code.

4.3 Results and Discussion

4.31 Radial reaction rate distribution

Radial fission and ^{10}B (n, α) rate traverses were measured with chambers in core 4A (Fig. 1) and in core 4B-1-1 which is a configuration of core 4B with seven sodium followers and one absorber rod inserted (Fig.2).

The experimental results of core 4A are compared with homogeneous and heterogeneous calculations in Fig. 7. All values are normalized to 1 at core centre. In addition to the rate distribution the ratio of calculated to measured rates was plotted on the right side of the figure using a suppressed ordinate scale to show the deviations more clearly.

In the driver zone, the homogeneous calculation underpredicts the fission rates in ^{235}U up to 10%, and in ^{239}Pu up to 15%. The heterogeneous calculation gives a softer spectrum (Fig.16), which enhances the calculated fission rates; in the driver zone this increase is in part cancelled by stronger self-shielding for ^{235}U , but not for ^{239}Pu . Thus, the fission rate in ^{235}U is underpredicted by at most 4%, in ^{239}Pu it is overpredicted in a part of the driver zone up to 7%. The calculated fission rate in ^{238}U agrees well with experiment in both cases.

In addition to this behaviour in the driver zone the ratios of calculated to measured fission rate of ^{235}U and ^{239}Pu shows strong fluctuations at the interfaces testzone-driver and driver-reflector, and go down in the reflector and blanket. Whereas the first effect is due to both experiment (averaged over the length of the chamber) and calculation (diffusion approximation is poor near boundaries), the second effect indicates that the flux distribution in the reflector and in the blanket is calculated too low.

The measured and calculated ^{10}B chamber traverse is compared in Fig. 8. The rate in the driver zone is overpredicted up to 12% by the homogeneous calculation, and up to 40% by the heterogeneous calculation. In interpreting these results, one must be aware that neutron streaming occurs along the channel (see chapter 4.11). Low energy neutrons streaming from the driver into the test zone increase the measured reaction rate in the test zone. This effect probably accounts for most of the discrepancy between heterogeneous calculation and experiments.

In core 4B-1-1 the radial traverses were measured in such a way that the channel passed the neighbourhood of 2 control rod positions, one of them occupied by the sodium follower and the other by the poison part (B_4C) of the rod (see Fig. 8). The agreement between experimental and theoretical fission rates is about the same as in core 4A with the homogeneous calculation, except that no large discrepancies are found at the test zone - driver interface. In the outer part of the driver all fission rates are underpredicted both near the boron rod and the sodium follower. The deviations are relatively small ($< 10\%$) for ^{235}U and ^{238}U and somewhat larger ($< 20\%$) for ^{239}Pu . The calculated $^{10}\text{B}(n,\alpha)$ rate shows good agreement with experiment in the core half with the inserted control rod. Note that there is not such a strong gradient of the reaction rate as in core 4A. Near the sodium follower the rate is overpredicted by about 10%. As in core 4A, both the experiment and the homogeneous calculation are probably in error.

Reaction rate distributions were also measured in the breeder blanket (see chapter 3.34). For this purpose uranium foils were irradiated in the outer part of the driver zone and in the sector of breeder blanket elements in core 4B-2 at two levels: 15 cm above and 15 cm below the core midplane. The results of these measurements are compared with homogeneous calculations in Fig. 9. The curves are normalized at the innermost points. The shape of the ^{238}U fission rate distribution at the level intersecting the sodium part of the rods is very well calculated while the calculated ^{235}U fission and ^{238}U capture rates at this level fall off more slowly in the blanket than the experimental values. In the outer row of blanket elements the discrepancy reaches the order of 10%. At the level intersecting the boron the agreement is very good for the ^{235}U fission and ^{238}U capture rate while the ^{238}U fission rate is underpredicted at the driver-blanket boundary by about 15%.

The calculated curves are taken from two XY-calculations with sodium and B_4C in the control rods, respectively (see chapter 2.4). The ratio of the rates of the 2 levels was taken from a RZ-calculation where the half inserted control rods were represented by a ring. This relatively poor approximation overestimated the rates at the B_4C level relative to that at the Na level by about 15%.

4.32 Rate distribution around control rods

The power profile near a control rod is a quantity of great interest in reactor design. Therefore uranium foils of 9.5 mm diameter were irradiated around a control rod. Fig. 10 shows that the experimental results are generally well predicted by calculations. An exception is the ^{235}U fission rate between the absorber rod and the reflector where the calculated value is about 15% too low. This is in agreement with the results of the ^{235}U chamber measurements in the same region (Fig. 7) which also gave results about 10% to 15% higher than those obtained by homogeneous calculations.

4.33 Axial rate measurements

The axial ^{239}Pu fission rate distribution was measured in SNEAK-4B-1 with Pu foils and PuO_2UO_2 plates. The technique of rate measurements with Pu foils is not yet fully developed at Karlsruhe. The experiments made in SNEAK-4 must be considered as a first step in this direction, aimed at looking into the problems of this technique rather than at producing a good rate traverse.

The results of the experiments are shown and compared with calculations in Fig. 11 (bottom left). As core 4B-1 is axially symmetric the figure was arranged so that in the left part the rates derived from plate activation in the right part those from foil activation are shown. All experimental data agree over 2/3 of the core height (+20 cm to -20 cm). Deviations are seen close to the core blanket interface indicating that the measured fission-induced γ -activity can only be considered proportional to the fission rate if the neutron spectrum causing the fissions is spatially constant.

If normalized in the centre ($Z=0$) the calculated and measured ^{239}Pu fission rates agree in the range $Z = -20$ cm to $+20$ cm within the experimental uncertainty. Outside this range the measurements with plates show smaller deviations from calculation than those with foils, the calculations always giving higher values.

Measurements with uranium foils were made in core 4B-2 in position 22/20 of the test zone and 17/17 of the driver zone. It can be seen from Fig. 10 that the maximum of the reaction rate distribution is shifted downward by about 5 cm in the test zone and 8 cm in the driver zone as a result of the half inserted control rods. The experimental data are compared to RZ-diffusion calculations in 26 energy groups with normalization at the rate maximum.

The experimental behaviour is well predicted in the test zone. In the driver position, the ^{235}U fission and ^{238}U capture rates in the poisoned upper core half are underpredicted by theory while the ^{238}U fission rate is overpredicted. The discrepancies reach up to 10% near the upper core blanket boundary. This indicates that the flux depression due to the B_4C absorber is overestimated in some parts of the neutron spectrum and/or the reflector efficiency of the axial blanket is underestimated in the diffusion calculations.

For comparison, calculations were repeated after condensation to 4 energy groups. This lead to a slight ($\sim 2\%$) increase of the deviations from experiment near the core blanket interface. Rates calculated in 4 groups using the control cell homogenization method showed a somewhat larger discrepancy in the upper core half. The boron influence on the rates is overestimated in this case because part of the boron is artificially brought closer to the axis of the rate calculation.

5. DOPPLER EFFECT

The Doppler effect was measured in SNEAK-4 using the hot versus cold sample oscillating technique. The flux signal was fed into an inverse kinetics program to determine the reactivity.

The measurements were carried out in the driver zone, which contributes most of the Doppler effect of the assembly. A sample of 25% enriched UO_2 was chosen because it matched the enrichment of the driver zone fuel as well as possible. The cylindrical sample was 9 cm high, 3.5 cm in diameter, and weighed 873.2 g. The sample and the experimental method is described by Barleon (ref. 13).

The method of analysis which includes the interaction between resonances in the hot sample and cold environment is described in (ref. 14). For ^{238}U the resolved resonance parameters by Garg (ref. 15) were used. The average parameters in the unresolved region were taken from J.J. Schmidt (ref. 16). Expansion effects were small and could be neglected. However, a correction for the crystal effects in UO_2 was applied using the phonon spectrum measured by Dolling (ref. 17).

In SNEAK-4A a series of measurements was made to investigate the dependence of the Doppler effect on the distribution of CH_2 around the sample. In the 8 elements around the pile-oscillator (position 17/17), the $(CH_2)_n$ foils were 1. distributed uniformly, 2. placed close to the pile oscillator, 3. placed away from the pile oscillator, as shown in the insert on the bottom left part of Fig. 12.

SNEAK-4A was close enough to symmetrical, so that the fluxes unperturbed by the sample could be obtained from one-dimensional diffusion theory calculations. The local flux depression factors were also calculated by diffusion theory, and applied to the unperturbed fluxes. The results of experiment and calculation are shown in Fig. 12. The agreement is satisfactory for the cases 1. and 2., where the calculation is about 10% too high. However, the predicted change to case 3. did not appear in the experiments, which gave about the same results for the cases 2. and 3.

For the KNK-II project it is important to know the Doppler effect per unit volume of driver zone material rather than the effect of a sample which is influenced by resonance interaction and by the flux depression in the sample. Therefore, the effect in the driver zone was calculated using the same method as for the analysis of the experiment. The resulting Doppler

reactivity at the position of the pile oscillator in the core midplane is shown on the top left part of Fig. 12. A comparison of these results with calculations carried out with the method used for KNK-II at INTERATOM using effective cross sections at different temperatures shows that the curves agree within 10%. Therefore, one can conclude that the Doppler coefficient in the KNK-II reactor can be predicted satisfactorily.

In order to determine the influence of a control rod on the Doppler effect an experiment was carried out in assembly 4B-1 close to a Na-follower and in 4B-3 close to a B_4C block (position 17/17, see Figs. 1 and 2). The results of experiment and calculation are shown on the top right part of Fig. 12. The agreement is satisfactory. Whereas the Na-follower has very little influence on the results, the B_4C absorber in the vicinity of the sample strongly reduces the Doppler effect.

A further set of measurements along an axial traverse near a half-inserted control rod was carried out in assembly 4B-2. The experimental results are shown on the bottom right part of Fig. 12. The presence of the absorber material influences the measurements in the upper half of the core. No calculations were made for this traverse because the geometry is too complicated.

The experimental values given in the figures could be determined with good accuracy and the statistical errors are small. On the other hand, the calculated values are influenced by uncertainties in the strongly transient spectrum, in the normalization integral, and in the effective delayed neutron fraction. As these uncertainties are rather large in a complicated assembly like SNEAK-4, it is surprising that the agreement between theory and experiments is as good as it is. However, a Doppler measurement is a highly integral experiment and there is undoubtedly some cancellation of errors.

6. NEUTRON SPECTRUM

6.1 Experimental Technique

In the centre of the core and in the driver zone of the assembly SNEAK-4A neutron spectrum measurements in the energy range from 1 eV to 6.5 MeV were performed. Three different experimental methods were used: in the energy range from 0.5 MeV to 6.5 MeV the Li^6 semiconductor sandwich spectrometer method (ref. 18), from 20 keV to 1.5 MeV the proton recoil technique (ref. 19), and from 1 eV to 600 eV the multiple foil (sandwich) method (ref. 20). The detectors used for these three techniques were placed at the same positions of the core. The neutron flux was measured during all experiments with a common monitor making possible an absolute adaption of the results obtained in the different energy ranges.

6.11 Semiconductor spectrometer

The neutron sensitive foil consisted of a $167 \mu\text{g}/\text{cm}^2$ thick Li^6F layer on a $15 \mu\text{g}/\text{cm}^2$ thick Vyns foil. As detectors for the charged particles silicon surface barrier counters with a sensitive area of 300 mm^2 and a thickness of $300 \mu\text{m}$ were used. The electronic discrimination against γ -pile-up processes in the detectors was performed by a fast-slow-coincidence circuit with cutting levels for the pulse height corresponding to 1.2 MeV (ref. 18).

The background pulse spectrum, resulting from (n,α) - and (n,p) -processes in the silicon of the detectors, was obtained by an additional measurement without the Li^6F -foil. For the energy calibration a $^{233}\text{U}-\alpha$ source on a Vyns foil was used. The energy resolution of the spectrometer was about 20% for 1 MeV neutrons and 10% for 2 MeV neutrons. The statistical error in the energy range below 2 MeV is <3% and increases up to 8.5% at 4 MeV and up to 22% at 6 MeV. The absolute cross section data for the $\text{Li}^6(n,\alpha)t$ reaction were taken from (ref. 21). Other measurements of the Li^6 cross section differ from these data by 10 to 15%.

6.12 Proton recoil spectrometer

One cylindrical counter (active length 7.4 cm, diameter 3.8 cm) filled with 3 atm. methane and three spherical counters (3.94 cm diameter) filled with 1, 2, and 4 atm. hydrogen, respectively, were used in the measurements.

The detectors were placed at the core midplane. About 900 cm³ of core material had to be removed to store detector and preamplifier (see Fig. 13). Below 50 keV the γ -n discrimination technique with an analog pulse height computer was used (ref. 19, 22).

The method of Benjamin (ref. 23) was used to correct the measured proton spectra for wall-effects, which furthermore were calculated by the Monte Carlo method. An energy calibration was provided by ²³⁹Pu α -particles and/or the 770 keV protons from the He³(n,p) reaction.

Energy calibration, energy resolution and the results of the Monte Carlo wall effect codes were checked with monoenergetic neutrons from the Li⁷(p,n)Be⁷ reaction. The protons for this reaction were produced from a van de Graaf accelerator.

The accuracy of the measurements, which in detail is discussed elsewhere (ref. 20), was estimated to be about +13% in the energy range above 50 keV. Problems with the γ -n discrimination technique below 50 keV arise from the heavily overloaded pulses caused by energetic protons. This may be the reason for systematic error in the evaluated spectrum below 50 keV.

6.13 Resonance activation foils in sandwich geometry

Because of the hardness of the spectrum in the test zone only 8 different resonance absorbers were found to be suitable to provide information about the lower energy region of the neutron spectrum. The flux values $\phi_m(u)$ at the energy of the main resonance of the absorber were obtained from the relation

$$\phi_m(u) = \frac{D}{\epsilon} \cdot \frac{P_m}{K_m} .$$

Here D is the measured difference of the saturation activity of the outer and inner foils of usually a three layer sandwich. The factor ϵ was determined by calibration in two well known spectra, the 1/E spectrum in the FRM reactor at München and a spectrum in the subcritical assembly SUAK which has been measured very carefully by the time-of-flight technique. P_m is the relative contribution of the main resonance to the total measured difference D. It could be calculated by means of a computer code from effective resonance integral data and an approximate spectrum. K_m is the calculated absolute self-shielding effect in the main resonance for unit flux. K_m can be written in the form of a difference of effective resonance

integrals of plane foils with different thicknesses (ref. 24). The effective resonance integrals needed for the evaluation of K_m were computed by means of the TRIX-1 code from the best resonance data known at the beginning of 1969.

In Table 10 the resonance absorbers used in the experiment and their characteristic data are listed.

All sandwiches activated in the SNEAK-4 core consisted of three foils except for Cd where 5 foils were used. The foils had a diameter of 18 mm and were covered by a Cd box with 0.5 mm wall thickness. The Cd boxes were placed in the Al 100% platelet of the cell in the test zone and in the Na_2CO_3 platelets of the cell in the driver zone.

The error margins of the results of the sandwich method in Fig. 13 contain the statistical errors, errors in the calculations of the resonance integrals and the contribution of higher resonances, and errors caused by the experimental equipment used.

6.2 Results and Discussion

The experimental results are compared in Fig. 13 with calculations in 2-dimensional diffusion theory using the 26 group NAP-PMB set (het.corrected). Experimental and theoretical results were normalized to equal integrals in the range from 21.5 keV to 1.4 MeV. This normalization yields a discrepancy of about 30% for the results of the Li^6 semiconductor method over the whole measured energy range. Therefore the results of the Li^6 measurements were also fitted by themselves to the theoretical curve adapting the integral spectrum in the range from 0.8 MeV to 6.5 MeV.

The comparison of the results obtained this way shows good agreement of experimental and calculated spectra in the energy range below 1keV and above 100 keV. Below 100 keV the calculation yields a higher flux than was measured by the proton recoil technique. This discrepancy is probably at least partly due to imperfections in the experimental technique: it was realized (ref. 20) that problems arise with the γ, n discrimination system especially at high count rates which disturb the proton spectrum. Therefore, the results obtained in this energy range are thought to be unreliable. Proton recoil and Li^6 measurements show a slight deviation from each other in the energy range below 800 keV.

7. MATERIAL WORTH MEASUREMENTS

7.1 Experimental Procedure

Reactivity worths for a number of samples were measured in the centre of the test zone (position 22/19) and in the driver zone (position 26/19) at core midplane using the horizontal drawer and the sample changer. The arrangement is shown in Fig. 5. The experimental reactivity worths were determined from the flux signal by solving the inverse kinetics equations on the DDP 124 computer. The results were corrected for linear reactivity drift between two reference measurements. The influence of the sample container and other structural materials was determined experimentally and eliminated. The experimental uncertainties given in Table 11 are mainly caused by statistics and non-linear drift effects.

7.2 Method of Calculation

The reactivity worths were calculated by perturbation theory applied to results of one-dimensional diffusion calculations in cylinder geometry. In addition to the usual first order perturbation program (FOP) an integral transport perturbation program (ITP) (ref. 33) was used. ITP is based on collision probabilities. It takes into account sample size effects including resonance self-shielding, treating the surrounding core and the sample as two homogeneous regions. All calculations were made with the 26 group NAP-PMB set.

7.3 Results and Discussion

The relevant information on the samples together with the experimental results is given in Table 11 while in Table 12 experimental and calculated values are compared. The following conclusions can be drawn from this comparison:

7.31 Central worths

Worths of absorbers are generally calculated too high, which is probably due to uncertainties in the normalization integral and in the effective delayed neutron fraction. This kind of disagreement is found in

most other critical assemblies. If the worths are normalized to that of ^{235}U the agreement is fairly good, except for ^{238}U which is calculated 25% too high. This indicates that there must be an error in the cross sections (σ_c too high, σ_f too low).

For Na, there is a large discrepancy and an even worse one for Al. In both cases the reactivity effect is a delicate balance between a negative effect at high energies and a positive effect at low energies.

For some of the samples there is very little difference between the calculations by FOP and ITP. However, ITP gives substantial improvement as compared to FOP for ^{238}U , Ta and Na. The sample size effect of ^{10}B is predicted only about half as large as measured. The reason should be in part that the spectrum in the centre is calculated too hard. This also explains that the worth of ^{10}B if normalized to ^{235}U is calculated about 10% too low.

7.31 Worths in the driver zone

Though there are strong spectral transients in the driver zone which probably cannot be well calculated the measured and calculated worths of absorber and fuel materials agree fairly well. However, there are large discrepancies for SS and Zr.

For Na and Al there is better agreement in the driver zone than in the centre. This probably is the case because the positive contribution of the low energy tail in this rather soft spectrum dominates, together with the positive leakage effect.

Again ITP gives better agreement for ^{238}U and Ta. The sample size effect of ^{10}B is predicted much better than for the central measurements.

8. PROMPT NEUTRON DECAY CONSTANT

8.1 Experimental Techniques

In SNEAK-4A, $\beta/1$ was measured by two independent methods, the pulsed source technique and the polarity correlation technique in the frequency domain.

8.11 Pulsed source technique

The neutron generator built by Eyrich is a 150 kV-Cockroft-Walton type accelerator with a duoplasmatron ion source (ref. 25, 26), using the D-T-reaction. The target is fixed at the end of a tube and introduced through the horizontal channel to a position near the centre of the core. The detector positions for two ^{235}U -fission chambers (20th Century Electronics type FC 165) were chosen in the core centre (position 20/20) and in the reflector (position 28/21) in order to detect possible space-dependent modes. In addition a ^{238}U chamber was used in the central position to check the time-dependence of the spectrum.

Within the error margins the experiment proved the existence of a time- and space-independent decay mode. In Fig. 13A the decay curves are plotted for the two different positions measured at 60 μ subcritical. After the initial higher modes have died out, there is good agreement in the further decay. Employing a least squares fit (ref. 27) α -values were obtained which are plotted in Fig. 13B versus the corresponding reactivities determined from control rod positions. The extrapolation to critical leads to $\alpha_c = 6500 \text{ s}^{-1}$ with an estimated error of $\pm 4\%$, extrapolation to prompt critical yields 1 β . This fact shows that the β_{eff} value for the rod calibration is consistent with the pulsed source measurements.

8.22 Polarity correlation technique

The newly developed cross correlation technique in the frequency domain (ref. 28) is especially suitable for measurements in fast reactors since the transfer function of the measuring equipment cancels out without calibration. From the coherence function $\rho(\omega)$, according to (ref. 28) α can be determined:

$$\alpha_c = \omega_c \cdot \sqrt{1 - \rho_0}$$

where ω_c is the break frequency and ρ_0 the amplitude at low frequencies (Fig. 13C). The experimental instrumentation in the reactor consisted of two sets of 2 ^3He -counters in the current mode, positioned at 20/20 and 22/20. In this case the ratio Q_{max} of correlated to uncorrelated noise is 2.02 and 1.85, respectively. The measuring time in the reactor was 11 minutes at 100 Watts. A multichannel magnetic tape recorder was used in the measurement. The value for the decay constant at critical was determined off-line as $\alpha_c = 7170 \text{ s}^{-1}$ with a statistical error somewhat less than 1%.

8.2 Calculations

The effective delayed neutron fraction, β_{eff} , and the lifetime of prompt neutrons, l , was obtained from one- and two-dimensional calculations based on homogeneous diffusion theory. The one-dimensional calculation of l was repeated with heterogeneity corrected cross sections. In all cases the NAP-PMB set was used. The delayed neutron parameters used are those of Keepin (ref. 29). The 26-group delayed neutron spectra were determined from publications of Keepin (ref. 29), Batchelor and Hyder (ref. 30), and Bonner et al. (ref. 31).

The calculated values are

$$\begin{aligned}\beta_{\text{eff},1d} &\approx \beta_{\text{eff},2d} &= 6.11 \cdot 10^{-3} \\ l_{1d,\text{hom}} &&= 5.83 \cdot 10^{-7} \text{ s} \\ l_{2d,\text{hom}} &&= 6.29 \cdot 10^{-7} \text{ s} \\ l_{1d,\text{het}} &&= 7.34 \cdot 10^{-7} \text{ s} .\end{aligned}$$

It can be seen that the calculational model has a strong influence on the neutron lifetime. Especially the plate structure in the driver region has a pronounced effect on l because it leads to a softening of the neutron spectrum relative to the homogeneous case: the neutron flux in the region below 1 keV is markedly increased (Fig. 16).

Extrapolation of the data to the two-dimensional heterogeneous case leads to

$$l_{2d,\text{het}}(\text{extrap.}) = 7.8 \cdot 10^{-7} \text{ s} .$$

Using this value the best calculated β/l value of the critical core SNEAK-4A is

$$\left(\frac{\beta}{\lambda}\right)_{\text{calc}} = \frac{\beta_{\text{eff}}}{\lambda_{2d,\text{het}}} = 7.800 \text{ s}^{-1} .$$

8.3 Discussion of the Results

The two experimental results show a discrepancy of about 10%. The increase in reactor size caused by counter balancing the large absorption by the ^3He -counters should not have such an effect. The pulsed source measurements clearly indicate the fundamental mode, and inaccuracies in the evaluation can also not be responsible for such a large error. On the other hand in the case of correlation technique the evaluation is based on the point reactor model. If this does not hold, i.e. if cross correlation and autocorrelation spectral densities depend in different ways on the geometry of the reactor, there is a systematic error. However, by now there is no clear explanation of the difference.

The ratio of calculated to experimental β/λ is 1.20 and 1.09 for the pulsed measurements and the correlation measurements, respectively. Assuming an experimental value of 6700 s^{-1} the ratio is 1.17. The discrepancy between experiment and calculation is thus in the same order of magnitude as previously observed in other critical assemblies. It is likely, that the discrepancy is due to a difference between experimental and calculated lifetime. One cause for this as pointed out by Kiefhaber (ref. 32) might be the use of the same group set for real and adjoint calculations.

9. SODIUM WORTH STUDIES

According to calculations of INTERATOM the reactivity change due to removal of sodium from parts of the core is always negative. This result was confirmed by two experiments:

- 1) Measurement of the reactivity worth of small sodium samples at the core centre and in the driver and
- 2) measurement of the reactivity change caused by voiding the sodium follower of a KNK-II control rod.

The results of the small sample measurements were already mentioned in chapter 7. Table 11 shows that the sodium worth at the core centre as well as in the driver position is positive corresponding to a negative void effect. The magnitude of the effect was underestimated by theory. The fact, that the sodium void effect is negative even in the core midplane where the leakage component is smallest guarantees an overall negative void effect.

The reactivity change due to voiding SNEAK elements was measured in two configurations of the core. In the first configuration the two outer and three inner sodium followers were in place. Here a sodium filled SNEAK element (Pos. 25/20) forming part of one of the inner sodium followers was replaced by an empty element. The measured reactivity change was -26.5 \textcent .

The second core configuration was that of SNEAK-4B-1 with 4 type 16 elements at the centre of the test zone. Here all four elements of the sodium follower (X=25-26; Y=20-21) were replaced by empty elements. The resulting reactivity change was -108 \textcent in good agreement with the result of the first measurement.

Because of the complex geometry no comparison with calculations was made. The experiments, however, showed that sodium voiding from a central rod channel would result in a large reactivity reduction.

10. USE OF SNEAK-4 RESULTS FOR THE KNK-II DESIGN

When planning the experimental program for SNEAK-4, four groups of experiments were regarded necessary in order to provide experimental information on the most important operational and safety characteristics of KNK-II. These four groups were:

- 1) Critical mass and reactivity values
- 2) Control rod worths
- 3) Doppler coefficient
- 4) Power distribution.

From the SNEAK-experiments on these four essential topics and from the calculations performed for the interpretation of these experiments the following conclusions for KNK-II can be drawn.

10.1 Critical Mass and Reactivity Values

10.11 The three-dimensional Monte Carlo code MOCA is the best available tool to calculate the multiplication factor k_{eff} of KNK-II. Analytical methods using diffusion theory codes require a number of corrections which at the moment cannot be obtained with high accuracy (S_N correction, streaming correction). The uncertainty of calculations with the MOCA code is about 0.6% in k_{eff} including a statistical error of $\pm 0.3\%$ (standard deviation) while the uncertainty is up to 1% in k_{eff} using analytical methods.

10.12 The results of MOCA and analytical calculations of k_{eff} are in good agreement. The discrepancies are well within the quoted uncertainty range.

10.13 Use of the KFK-NAP-PMB 26 group data library leads to an underprediction of k_{eff} by about 1.5%. The critical enrichment in the given core geometry of KNK-II should therefore be determined from a calculation with $k_{\text{eff}} = 0.985$.

10.14 Use of the 26 group MOXTOT set of KFK gives a significant improvement in the prediction of k_{eff} . Within the methodical error of the calculation the critical mass calculated with the MOXTOT set is in agreement with experiment. However, a comparison of MOXTOT calculations to a large number of critical assemblies with ^{235}U and ^{239}Pu as main fissile isotope leads to the conclusion that the good prediction for SNEAK-4 is due to the compensation of overreactive ^{235}U and under-reactive ^{239}Pu data (ref. 10). This conclusion is also supported by the comparison of fission and capture rates calculated with the NAP-PMB and MOXTOT set (Fig. 15). Normalized to unit integral fission source the capture rate of ^{238}U is about 10% lower, the capture rate of ^{239}Pu 7% higher, and the fission rate of ^{239}Pu 2 to 3% lower with the MOXTOT set, while the ^{235}U rates are nearly unchanged.

10.2 Control Rod Worth

~~10.21~~ ~~No direct measurements of control rod worths were possible since~~ the reactivity values were too large. In the experiments the shut-down effect of the rods had to be compensated by increasing the enrichment of the test zone. Thus only the sum of reactivity changes due to both procedures could be measured exactly. It can, however, be assumed that the calculated effect of enrichment changes deviates from the correct value about to the same extent as the calculated k_{eff} of a clean assembly, i.e. by a factor of ~ 0.985 . This is also supported by experiments (see chapter 3.4). With this assumption the difference of the ratios of k_{theor}/k_{exp} between the respective assemblies gives the absolute error of the calculated control rod worth.

10.22 The most important experiments with respect to KNK-II operation are SNEAK-4B-2 with 6 control rods half inserted and in comparison to this SNEAK-4B-1 with 8 Na-followers. These assemblies simulate the KNK-II reactor at the beginning and at the end of life. The difference in reactivity between both experiments is correlated to the worth of the bank of 6 absorbers. The relative deviation $(\rho_{calc} - \rho_{exp})/\rho_{exp}$ in this case is +6% with the cell method, -0.3% with the ring method, and $+(2.5 \pm 4)\%$ with the MOCA method. It may be stated, that within the experimental and calculational uncertainties all calculated rod worths are in agreement with experiment.

10.23 The same agreement is found for the reactivity worth of one, two, and three fully inserted control rods (see Table 7). Here the relative deviation $(\rho_{\text{calc}} - \rho_{\text{exp}}) / \rho_{\text{exp}}$ using 2-dimensional diffusion theory and appropriate transport and streaming corrections in all cases is within +5%.

10.3 Doppler Coefficient

10.31 Use of zirconiumhydride in the driver region of the KNK-II guarantees a negative Doppler effect of sufficient magnitude. Spatial rearrangement of the ZrH_x has only a relatively small effect on the Doppler coefficient.

10.32 The experimental Doppler effect is in good agreement with predictions made at Karlsruhe. A comparison of the Doppler effect per unit volume of driver zone material with calculations carried out by the method used for KNK-II at INTERATOM also shows agreement within about 10%.

10.33 One can conclude that the Doppler coefficient of KNK-II may be predicted with an uncertainty of about +20%.

10.4 Power Distribution

The fission rate distribution of SNEAK-4A and of SNEAK-4B-1-1 obtained by homogeneous calculations deviate considerably from the measured data. Heterogeneous calculations for SNEAK-4A show that a large part of these deviations is due to the SNEAK plate structure and has no bearing on the power reactor with its different and much more homogeneous fine structure.

There remain, however, deviations between the experimental and calculated ^{239}Pu fission rate near the test zone - driver interface and between the experimental and calculated ^{235}U fission rate near the driver - reflector interface. Diffusion theory calculations with a single multigroup set will thus lead to erroneous predictions of the power distribution at these interfaces with deviations in the order of 5%. The direction of the deviation is

such, that the actual power is higher than calculated in the outer parts of the test zone and of the driver. In KNK-II this might lead to a slight additional power flattening.

10.5 Further Results Obtained from the Critical Experiment

10.51 The results of material worth measurements give some indications of possible errors in the integral cross sections of single isotopes. They will be valuable for detailed investigations of the effect of the difference in isotopic composition between KNK-II and SNEAK-4 and for estimating the resulting uncertainties of predictions for KNK-II. The material worth measurements of sodium can be considered to be a direct experimental check on the sodium void coefficient which is confirmed to be negative even at the core centre.

10.52 β/l is calculated about 17% high even with a two-dimensional treatment using heterogeneity corrected cross sections. It is calculated more than 50% high with a simple 1-dimensional calculation using homogeneous cross sections.

10.53 Power distributions in blanket elements which may possibly be inserted into KNK-II at the outer core boundary can be calculated well within an accuracy of a few percent.

ACKNOWLEDGEMENT

Many people both at Karlsruhe and INTERATOM have contributed to the work reported in this paper. The authors especially like to acknowledge the cooperation of the SNEAK operation group and contributions of F.W.A. Habermann, F.Helm, G. Jourdan, and H. Walze.

References:

- Ref. 1 D. Eitner et al., Physics Considerations in Design and Mock-up Experiments on SNEAK for KNK II, Proceedings of the BNES Conf. on "The Physics of Fast Reactor Operation and Design", London 1969, paper no. 2.1
- 2 P. Engelmann et al., Fast Reactor Physics Vol. II, p. 35, IAEA, Vienna 1968
- 3 J. Lieberoth, Nukleonik 11, 213 (1963)
- 4 D. Wintzer, Report KFK-743 (1969)
- 5 R. Bonalumi, Energia Nucleare 15, 608 (1968)
- 6 L.P. Abagjan et al., KFK-tr-144 (translation)
-
- 7 H. Huschke, Report KFK-770 (1968)
- 8 H. Küsters et al., Fast Reactor Physics Vol. I, p. 167, IAEA, Vienna 1968
- 9 K.H. Beckurts et al., Fast Reactor Physics Vol. 1, p. 67, IAEA, Vienna 1968
- 10 E. Kiefhaber et al., Evaluation of Fast Critical Experiments by Use of Recent Methods and Data, Proceedings of the BNES Conf. on "The Physics of Fast Reactor Operation and Design", London 1969, paper no. 1.9
- 11 H. Seufert and D. Stegemann, Nucl. Sci. and Eng. 28, 277 (1967)
- 12 R. Böhme and H. Seufert, Report KFK-811 (1968)
- 13 L. Barleon, report in preparation
- 14 E.A. Fischer, Report KFK-844 (1969)

- Ref. 15 J.B. Garg et al., Phys. Rev. 134, B 985 (1965)
- 16 J.J. Schmidt, Report KFK-120 (1966)
- 17 G. Dolling et al., Can. Journal of Phys. 43, 1397 (1965)
- 18 H. Bluhm and D. Stegemann, Theoretical and Experimental Investigations for an Improved Application of the Li⁶ Semiconductor Sandwich Spectrometer, to be published in Nucl. Instr. and Methods
- 19 E.F. Bennet, Nucl. Sci. and Eng. 27, 16 (1967)
- 20 H. Bluhm et al., Neutron Spectrum Measurements in Various SUAK Assemblies, Proceedings of the BNES Conf. on "The Physics of Fast Reactor Operation and Design", London, 1969, paper no. 1.5
- ~~21 E.D. Pendelbury, Report AWREO-60/64 (1964)~~
- 22 M.G. Strauss and R. Brenner, Rev. Sci. Instr. 36, 1857 (1965)
- 23 P.W. Benjamin, C.D. Kenshall, and J. Redfern, Report AWRE 2/64 (1964)
- 24 T.J. Connolly, F. de Kruijf, J.J. Schmidt, Report KFK-718 (1968)
- 25 M. von Ardenne, Tabellen der Elektronenphysik, Ionenphysik und Übermikroskopie, VEB-Verlag, Berlin 1956
- 26 W. Eyrich and A. Schmidt, Pulsed Neutron Research Vol. II, p. 589, IAEA, Vienna 1965
- 27 H. Spaeth, Report KFK-707 (1968)
- 28 W. Seifritz, The Polarity Correlation of Reactor Noise in the Frequency Domain, to be published in Nucl. Appl.
- 29 G.R. Keepin, Physics of Nuclear Kinetics, p. 86, 87, 94, Addison Wesley Publ. Co. (1965)

- Ref. 30 R. Batchelor and H.R. Machyder, J. of Nucl. Energy 3, 7 (1956)
- 31 T.W. Bonner, S.J. Bame, J.E. Evans, Phys. Rev. 101, 1514 (1956)
- 32 E. Kiefhaber, Report KFK-882 (1968)
- 33 E.A. Fischer, Report KFK-995 (1969)

Table 1: Composition of Elements Used in SNEAK 4
(Atom Density in 10^{21} atoms/cm³)

Isotope	Type 3	Type 11	Type 12, core	Type 12, 18, 19, 19-3 reflector	Type 13, core	Type 14, core	Type 16, core	Type 17, core	Type 20, 13-17, 24 reflector
Al	-	-	2.0978	-	3.1787	6.3533	7.5641	7.5641	0.006
C	0.0136	0.1976	3.9151	0.096	0.0468	0.0431	0.0474	0.0474	0.0562
Cr	1.196	15.986	4.3106	7.5452	2.8481	2.5134	3.0667	3.0667	3.0447
Fe	3.9549	54.089	14.573	25.53	9.6093	8.7646	10.2667	10.2667	10.333
H	-	-	3.3163	-	-	-	-	-	0.2588
Mg	-	-	0.0166	-	0.0345	0.0669	0.0794	0.0794	0.00266
Mo	0.0184	0.3004	0.0462	0.1185	0.0209	0.0279	0.0341	0.0341	0.0221
Na	-	-	10.732	11.0036	8.3241	6.2435	2.0733	2.0733	8.3053
Nb	-	0.0085	0.0085	0.0085	0.0087	0.0087	0.0087	0.0087	0.0087
Ni	0.9845	7.2838	2.1983	3.7033	1.5888	1.4742	1.6709	1.6709	1.651
O	-	-	6.7889	-	12.25	12.25	12.204	12.204	17.426
Pu239	-	-	-	-	1.4788	1.4788	1.4734	1.4734	-
Pu240	-	-	-	-	0.13285	0.13285	0.13236	0.13236	-
Pu241	-	-	-	-	0.01207	0.01207	0.012029	0.012029	-
Pu242	-	-	-	-	0.0006	0.0006	0.0006	0.006	-
Si	0.0455	0.618	0.2592	0.3952	0.2255	0.2227	0.2107	0.2107	0.2129
Ti	-	0.277	0.0324	0.0944	-	-	0.0177	0.0177	-
U235	0.1624	-	1.7892	-	0.92893	1.8250	3.2184	3.6038	0.06223
U238	39.94	-	3.2781	-	6.1052	7.7475	11.378	10.990	8.5805

Table 1: Composition of Elements Used in SNEAK 4 (continued)
 (Atom Density in 10^{21} atoms/cm³)

Isotope	Type 21, 22 core	Type 24 core
Al	13.430	0.0033
C	2.2588	2.2958
Cr	4.5070	3.3302
Fe	15.125	11.819
H	4.4112	-
Mg	0.1108	-
Mo	0.0422	-
Na	-	10.7256
Ni	2.2076	1.9218
O	-	11.506
Pu239	-	1.7389
Pu240	-	0.4356
Pu241	-	0.1479
Si	0.4128	-
Ti	0.0802	-
U235	2.5715	3.8065
U238	5.9446	1.0634

Isotope	Type 18, 19-3 lower part	Type 19, 19-3 upper part
Al	-	0.5042
B10	-	9.4494
B11	-	38.762
C	0.0432	12.096
Cr	3.17	2.5524
Fe	10.728	8.2928
Mg	-	0.0174
Mo	0.0245	0.00997
Ni	1.8453	1.1756
Si	0.1726	0.1718
Ti	-	0.0369
Na	16.61	-

Table 2: Comparison of the Composition of SNEAK-4 and KNK-II

Isotope	Atomic Density in 10^{21} atoms/cm ³				SNEAK-4, Type 24	SNEAK-4, Type 12
	Testzone KNK-II	SNEAK-4 Type 24	Driverzone KNK-II	SNEAK-4 Type 12	Testzone KNK-II	Driverzone KNK-II
Cr	2.950	3.302	2.950	4.3106	1.119	1.461
Fe	11.74	11.819	11.74	14.573	1.007	1.241
Ni	2.059	1.9218	2.059	2.1983	0.933	1.068
Na+Al	10.65	10.789	10.65	12.8298	1.013	1.205
O+C	12.81	13.818	10.68	10.704	1.079	1.002
H	-	-	3.297	3.3163	-	1.006
U235	3.699	3.8065	1.727	1.7892	1.029	1.036
U238	0.7847	1.0634	3.611	3.2781	1.355	0.908
Pu239	1.747	1.7389	-	-	0.995	-
Pu240	0.1576	0.4536	-	-	2.878	-
Pu241	0.01653	0.1479	-	-	8.947	-

Table 3: Group Structure of the 26 Group and 4 Group Sets

4 Groups	26 Groups	Energy Boundaries			Δu	
I	1	6.5	-	10.5	MeV	0.48
	2	4.0	-	6.5	"	0.48
	3	2.5	-	4.0	"	0.48
	4	1.4	-	2.5	"	0.57
	5	0.8	-	1.4	"	0.57
II	6	0.4	-	0.8	"	0.69
	7	0.2	-	0.4	"	0.69
	8	0.1	-	0.2	"	0.69
	9	46.5	-	100	keV	0.77
	10	21.5	-	46.5	"	0.77
III	11	10.0	-	21.5	"	0.77
	12	4.65	-	10.0	"	0.77
	13	2.15	-	4.65	"	0.77
	14	1.0	-	2.15	"	0.77
IV	15	465	-	1000	eV	0.77
	16	215	-	465	"	0.77
	17	100	-	215	"	0.77
	18	46.5	-	100	"	0.77
	19	21.5	-	46.5	"	0.77
	20	10.0	-	21.5	"	0.77
	21	4.65	-	10.0	"	0.77
	22	2.15	-	4.65	"	0.77
	23	1.0	-	2.15	"	0.77
	24	0.465	-	1.0	"	0.77
	25	0.215	-	0.465	"	0.77
	26		0.025		"	0.77

Table 4: Description of Elements Used in SNEAK-4

Type	Composition	Height, cm
3	Rods of depleted uranium	152.5
11	rods and blocks of stainless steel	101.6
12,13	see fig. 3	see fig. 3
14,16,17	see fig. 3	same as type 13
18,19,19-3	see fig. 4	see fig. 4
20	platelets (6.28 mm thick) of Na and UO ₂ alternately	101.6
21,22	see fig.4	see fig. 4
24	see fig. 3	see fig. 3

Table 6: Change in Reactivity Caused by Change in Enrichment of a Central Fuel Element in SNEAK-4B-1 (see Fig. 1)

Replacement	Method of Calculation	Change in Reactivity Δk		β_{eff} used	$\frac{\Delta k_{calc}}{\Delta k_{meas}}$
		calculated %	measured %		
Type 14 replaced by type 13	1-d perturbation	-0.173	-0.155	$6.01 \cdot 10^{-3}$	1.11
	1-d diffusion	-0.195			1.26
Type 14 replaced by type 16	1-d perturbation	+0.253	+0.302	$6.01 \cdot 10^{-3}$	0.837
	1-d diffusion	+0.294			0.975

Table 9: Simulation of a Radial Breeder Blanket (see Fig. 2)

Assembly	$k_{eff, meas}$	Δk	β_{eff} used
SNEAK-4B-2	1.00651	-0.00135	$5.85 \cdot 10^{-3}$
SNEAK-4B-2 with 13 type 20 elements	1.00516		$5.85 \cdot 10^{-3}$

Table 5: k_{eff} of the SNEAK-4 Assemblies
(see Figs. 1 and 2)

Assembly	Method of Calculation	$k_{eff,calc}$ ⁺⁾	$k_{eff,meas}$	β_{eff} used	$k_{eff,calc}$
					$k_{eff,meas}$
SNEAK-4A	2-d (x,y) diffusion S4 ZERA	0.971 +0.015 <u>+0.007</u> 0.993	1.0056	$6.11 \cdot 10^{-3}$	0.987
	MOCA ZERA	0.986 <u>+0.007</u> 0.993			0.987
SNEAK-4B-1	2-d (x,y) diffusion S4 ZERA STREAMING	0.956 +0.020 +0.005 <u>+0.005</u> 0.986	1.0007	$6.01 \cdot 10^{-3}$	0.985
	MOCA ZERA	0.981 <u>+0.005</u> 0.986			0.985
SNEAK-4B-2	2-d (r,z) diffusion S4 ZERA STREAMING	0.963 +0.023 +0.004 <u>+0.002</u> 0.992	1.0065	$5.85 \cdot 10^{-3}$	0.986
	MOCA ZERA	0.986 <u>+0.004</u> 0.990			0.984
SNEAK-4B-3	2-d (x,y) diffusion S4 ZERA STREAMING	0.967 +0.022 +0.004 <u>+0.002</u> 0.995	1.0060	$5.85 \cdot 10^{-3}$	0.989
	MOCA ZERA	0.996 <u>+0.004</u> 1.000			0.994

⁺⁾ Standard deviation for all MOCA results 0.003

Table 7: Simulation of KNK-II Control Rods (see Figs. 1 and 2)

Assembly	Method of Calculation	$k_{\text{eff,calc}}$	$k_{\text{eff,meas}}$	$\beta_{\text{eff used}}$	$\frac{k_{\text{eff,calc}}}{k_{\text{eff,meas}}}$	Exp. Rod Worth
SNEAK-4B-1	2-d (x,y) diffusion S4 ZERA STREAMING	0.956 +0.020 +0.005 <u>+0.005</u> 0.986	1.0007	$6.01 \cdot 10^{-3}$	0.985	
SNEAK-4B-1-1 (1 control rod)	2-d (x,y) diffusion S4 ZERA STREAMING	0.966 +0.020 +0.005 <u>+0.004</u> 0.995	1.0102	$5.95 \cdot 10^{-3}$	0.984	2.38%
SNEAK-4B-1-2	2-d (x,y) diffusion S4 ZERA STREAMING	0.956 +0.021 +0.005 <u>+0.004</u> 0.986	1.0003	$5.95 \cdot 10^{-3}$	0.985	
SNEAK-4B-1-3 (2 control rods)	2-d (x,y) diffusion S4 ZERA STREAMING	0.968 +0.022 +0.005 <u>+0.003</u> 0.998	1.0108	$5.89 \cdot 10^{-3}$	0.987	+2.63% <u>5.01%</u>
SNEAK-4B-3 (3 control rods)	2-d (x,y) diffusion S4 ZERA STREAMING	0.967 +0.022 +0.004 <u>+0.002</u> 0.995	1.0060	$5.85 \cdot 10^{-3}$	0.989	+2.19% <u>7.20%</u>
SNEAK-4B-2 (6 half-inserted rods)	see Table 5					7.15%

Table 8: SNEAK Elements with KNK-II Composition (see Fig. 1)

Assembly	Method of Calculation	$k_{\text{eff,calc}}$	Δk_{calc}	$k_{\text{eff,meas}}$	Δk_{meas}	$\beta_{\text{eff used}}$	$\frac{\Delta k_{\text{calc}}}{\Delta k_{\text{meas}}}$
SNEAK-4B-1	2-d diffusion	0.956		1.0007		$6.01 \cdot 10^{-3}$	
	S4	+0.020					
	ZERA	+0.005					
	STREAMING	<u>+0.005</u>					
		0.986					
			<u>+0.009</u>		<u>+0.0106</u>		<u>0.850</u>
SNEAK-4B-1 with 4 central type 24 elements	2-d diffusion	0.964		1.0113		$6.01 \cdot 10^{-3}$	
	S4	+0.021					
	ZERA	+0.005					
	STREAMING	<u>+0.005</u>					
		0.995					

Table 10: Properties of Resonance Absorbers Used as Sandwich Spectrometers

Isotop	Number of resolved Resonances with $I=0$ below 100 keV	Form	Thickness μ	Driver Zone			Test Zone		
				Energy	rel.diff. D, %	$P_m, \%$	Energy	rel.diff. D, %	$P_m, \%$
Cu63	31	metal	100	576	6.9	88.0	576	2.4	77.1
Mo98	8	metal	200	467.2	3.7	60.0	467.2	1.8	42.6
Mn55	35	metal +12%Ni	50	337	5.1	74.8	337	2.2	53.2
Cd114	6	metal	500	120.2	2.6	37.3	394.1	0.8	7.9
Br81	3	KBr	500	101	12.0	33.7	135.5	2.5	8.7
La139	69	metal	250	72.4	8.5	93.5	72.4	1.4	28.3
W186	27	metal	25	18.8	17.7	95.1	18.8	3.0	30.1
Au197	50	metal	25	4.91	14.5	74.3	293.4	1.9	10.1

Table 11: Experimental Material Worths in SNEAK-4A ($\$/\text{kg}\cdot 10^3$)

Material	Material Weight, g	Side Length of Square Sample, cm	Thickness ¹⁾ cm	Central Worth ⁴⁾	Driver Zone Worth ⁴⁾	Remarks
Al	36.08	4.665	0.628	3.0 \pm 1.5	51 \pm 1	
B10	0.085	4.665	0.63	-14000 \pm 800	-26000 \pm 1000	in Al container
B10	0.307	4.665	0.63	-13300 \pm 300	-22100 \pm 200	in Al container
B10	0.396	4.665	0.63	-12500 \pm 100	-18380 \pm 60	in Al container
Na	11.78	5.068	0.628	24 \pm 7	82 \pm 5	in SS container
Pu239	1.484	4.665	0.325	830 \pm 60	-	Pu-Al in Al
PuO ₂ UO ₂ ²⁾	135.81	5.068	0.628	189.8 \pm 0.3	-	in SS container
SS	108.9	4.665	0.628	-16 \pm 0.6	10.3 \pm 0.6	
Ta	53.74	4.665	0.15	-181 \pm 1	-243 \pm 1	
U235	3.425	4.665	0.011	543 \pm 20	342 \pm 20	
U238	61.67	4.665	0.157	-17 \pm 1	-18 \pm 1	
Zr	23.40	5.068	0.628	-	55 \pm 2	in SS container
ZrH _{1,7}	44.58	5.068	0.628	-	305 \pm 1	in SS container
Zr/ZrH _{1,7} ³⁾	32.50	5.068	0.628	-	180 \pm 2	

1) including sample container; 2) composition of PuO₂UO₂ sample in grams 3) 50 w/o Zr + 50 w/o ZrH_{1,7}

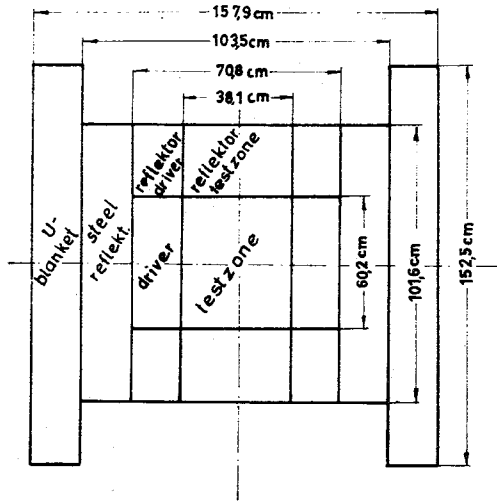
U235	U238	Pu239	Pu240	Pu241	016
0.63	87.3	29.05	2.64	0.27	15.92

4) the reactivity effect of the sample container is subtracted using experimental data

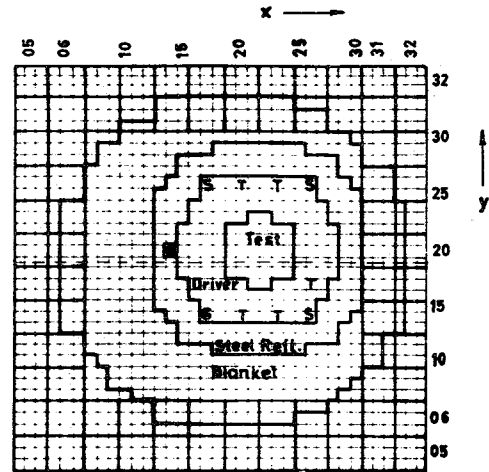
Table 12: Comparison of Experimental and Calculated Material Worth
in SNEAK-4A ($\beta_{\text{eff}} = 6.11 \cdot 10^{-3}$)

	Central Worth		Driver Zone	
	Calc/Exp		Calc/Exp	
	<u>FOP</u>	<u>ITP</u>	<u>FOP</u>	<u>ITP</u>
Al	-2.7	-2.3	0.73	0.74
B10 (0.085 g)	1.01	1.01	1.12	1.08
B10 (0.307 g)	1.07	1.05	1.31	1.14
B10 (0.896 g)	1.13	1.08	1.58	1.19
Na	0.34	0.54	0.62	0.63
Pu239	1.07	1.09	-	-
PuO ₂ UO ₂	0.98	1.14	-	-
Ta	1.52	1.15	3.1	1.25
SS	1.25	1.12		0.26
U235	1.15	1.14	1.05	1.03
U238	1.59	1.41	1.63	1.14
Zr			0.04	0.07
ZrH _{1,7}			0.83	0.90
Zr/ZrH _{1,7}			0.23	0.60

SNEAK-4 A

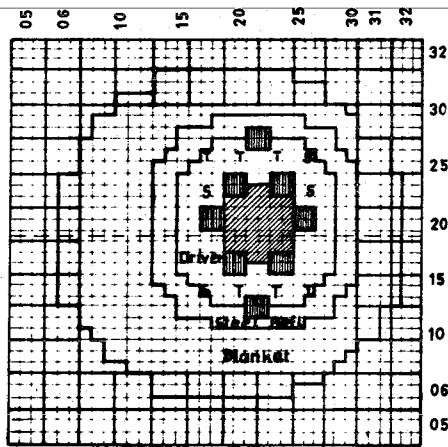


SNEAK-4 A



Testzone: Type 13 Elements

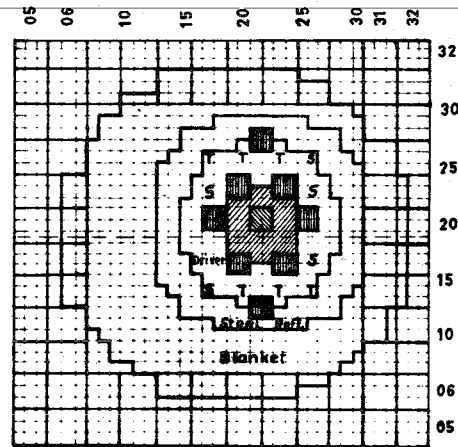
SNEAK-4B-1



▨ Type 14 Elements
 ▩ Type 18 Elements

S = Safety Rod
 T = Shim Rod
 R = Fine Control Rod

SNEAK-4B-1
 with 4 central elements
 with KNK-II composition

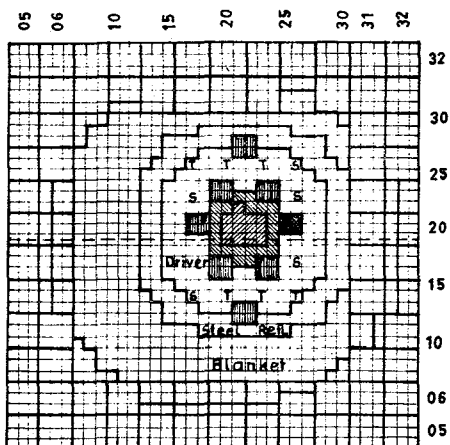


▨ Type 14 Elements
 ▩ Type 24 Elements
 ▩ Type 18 Elements

SS Reflector = Type 11 Elements
 Blanket = Type 3 Elements
 Driverzone = Type 12 Elements

Fig.1 Geometry of SNEAK Assemblies: Vertical and Horizontal Cross Sections of 4A and 4B-1

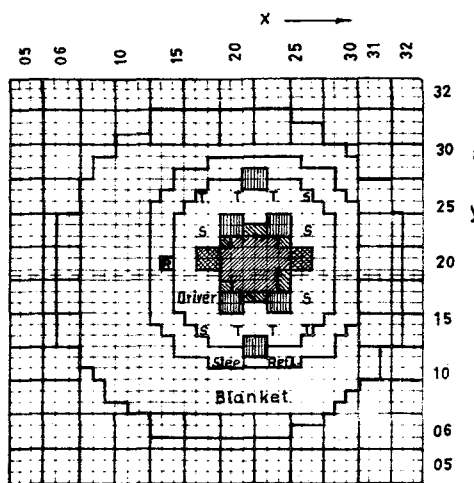
SNEAK-4B-1-1
and 4B-1-2*



- Type 16 Elements
- Type 14 Elements
- Type 19 Elements
- Type 18 Elements

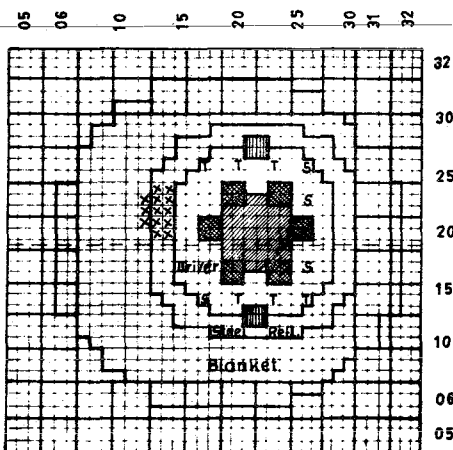
* Type 19 Element in Position 18/21

SNEAK-4B-1-3



- Type 16 Elements
- Type 14 Elements
- Type 19 Elements
- Type 18 Elements

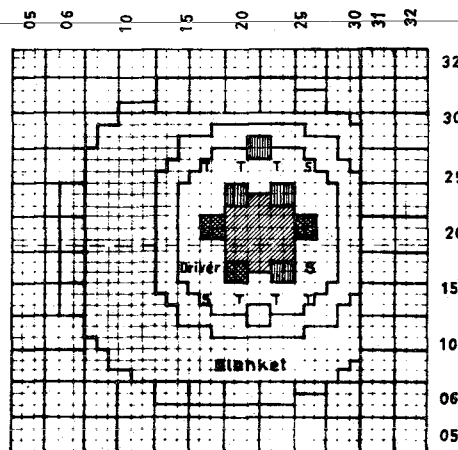
SNEAK-4 B-2



- Type 16 Elements
- Type 19-3 Elements
- Type 18 Elements
- *** KNK II Blanket

R = Fine Control Rod
S = Safety Rod
T = Shim Rod

SNEAK-4B-3



- Type 12 Elements
- Type 18 Elements
- Type 19 Elements

Driverzone = Type 12 Elements
SS Reflector = Type 11 Elements
Blanket = Type 3 Elements

Fig.2 Geometry of SNEAK-4 Assemblies: Horizontal Cross Section of 4B-1-1, 4B-1-2, 4B-1-3, 4B-2 and 4B-3

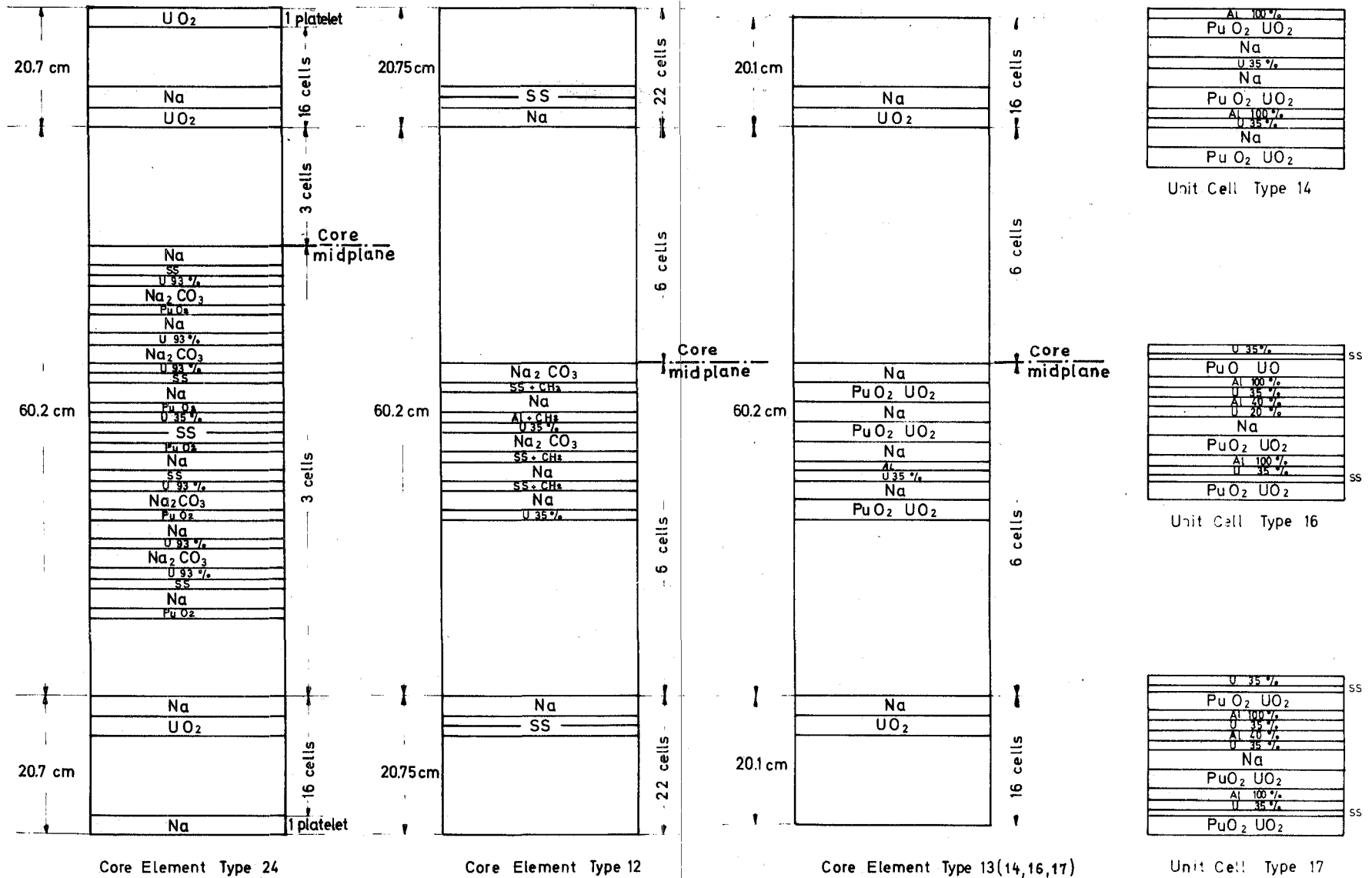


Fig.3 Loading Schemes of the Basic Elements Used in the SNEAK-4 Assemblies, Part 1

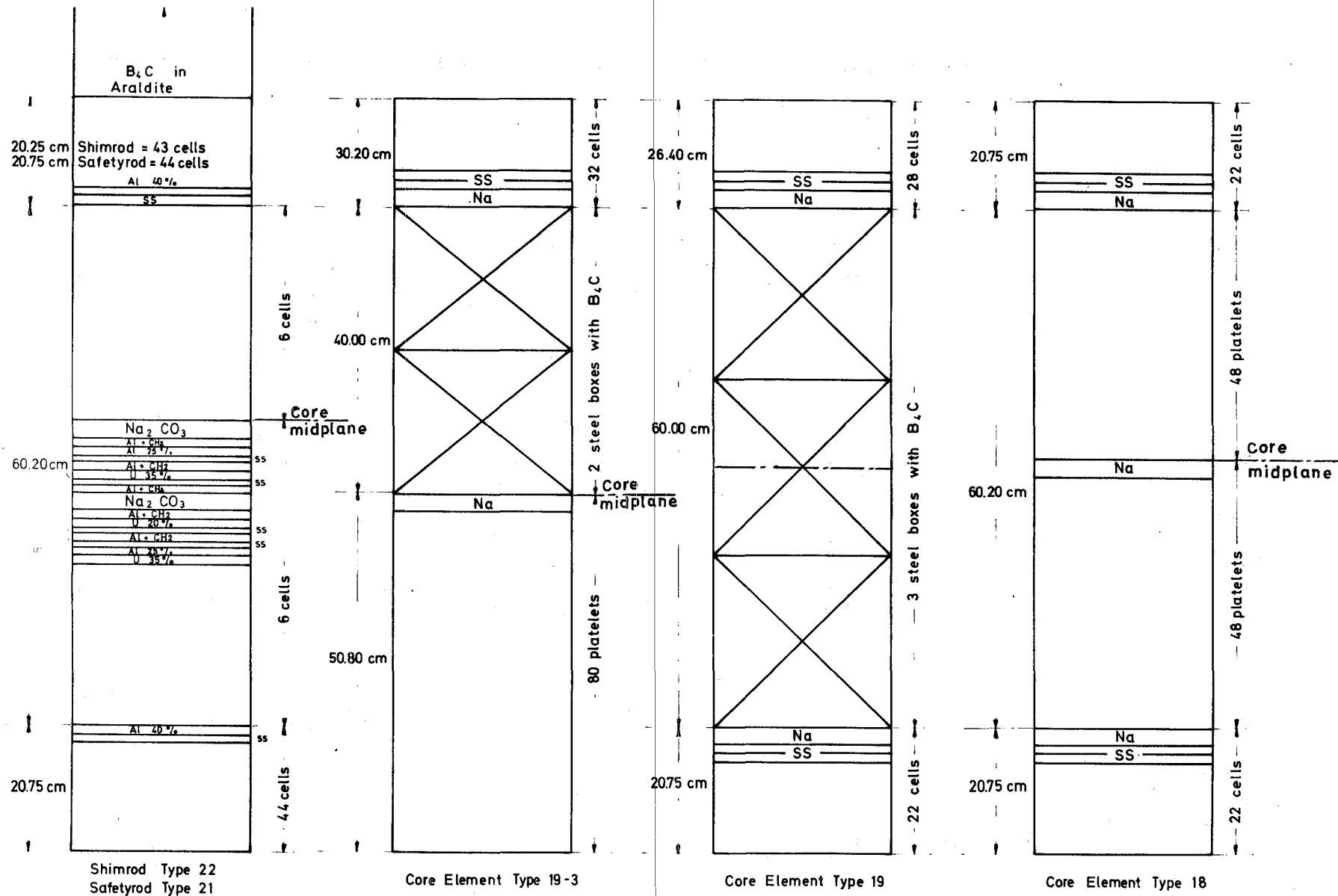


Fig.4 Loading Schemes of the Basic Elements Used in the SNEAK-4 Assemblies, Part 2

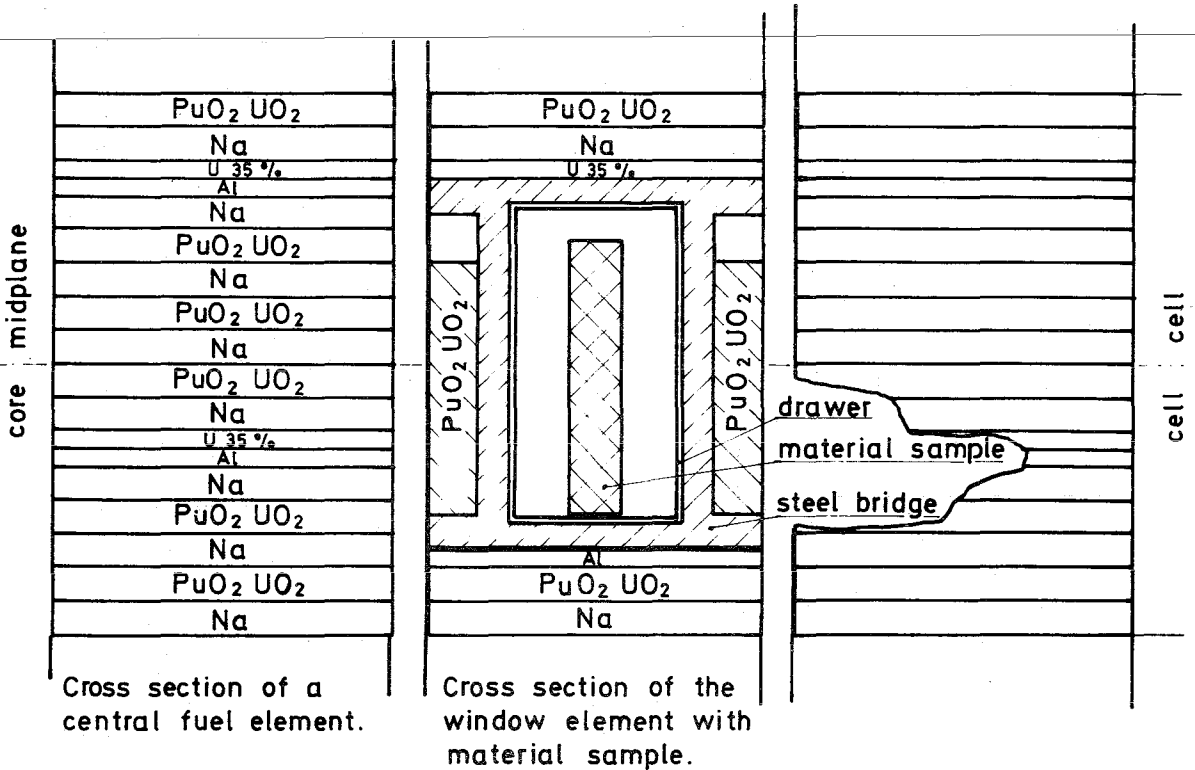
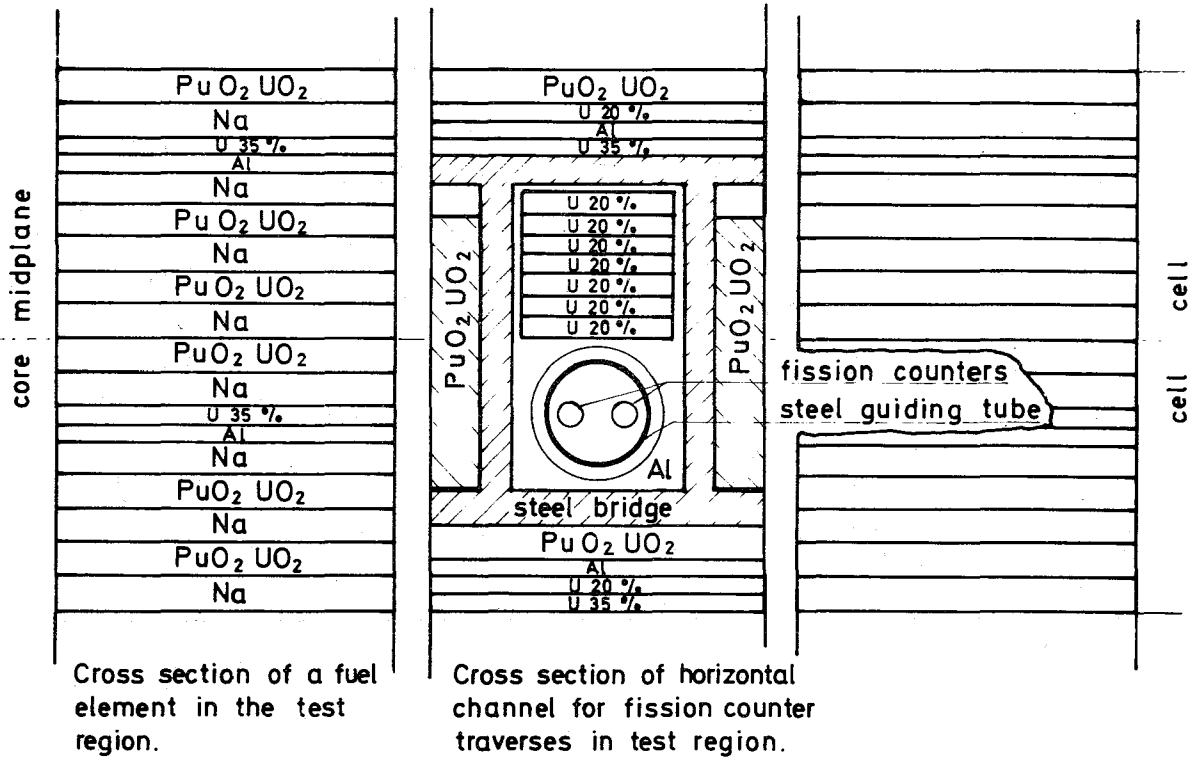


Fig.5 Plate Arrangement around Horizontal Channel for Chamber Traverses and Material Worth Measurements

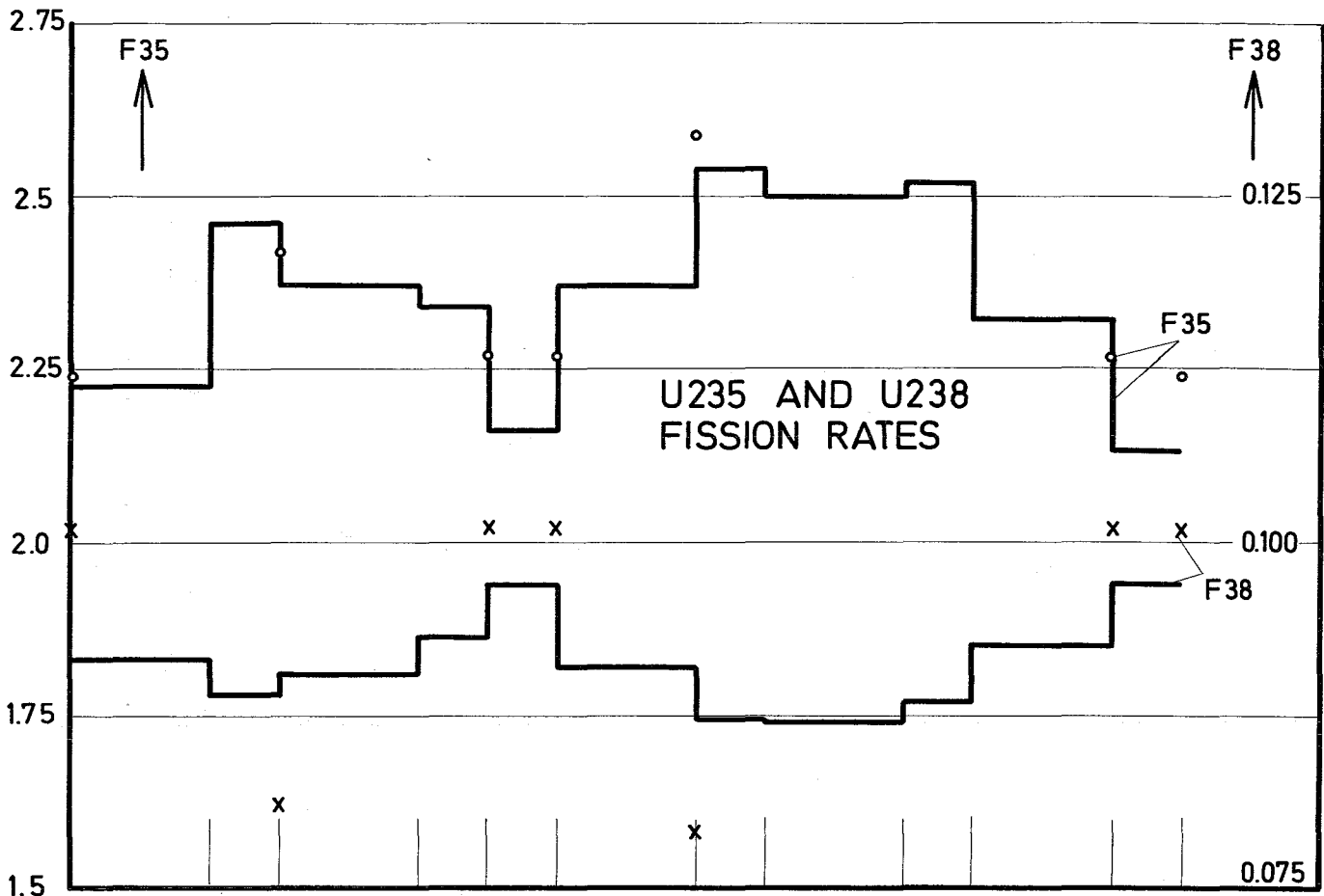
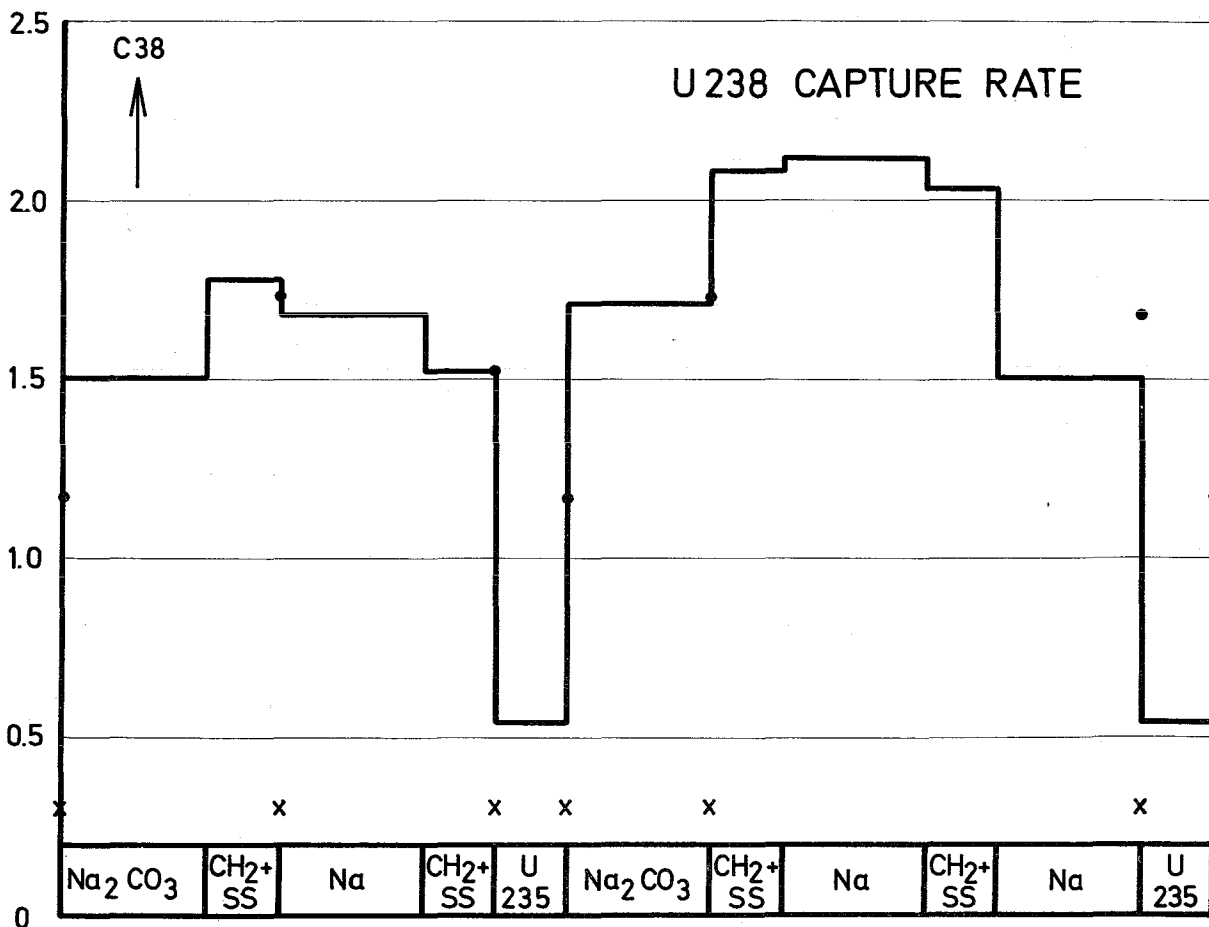
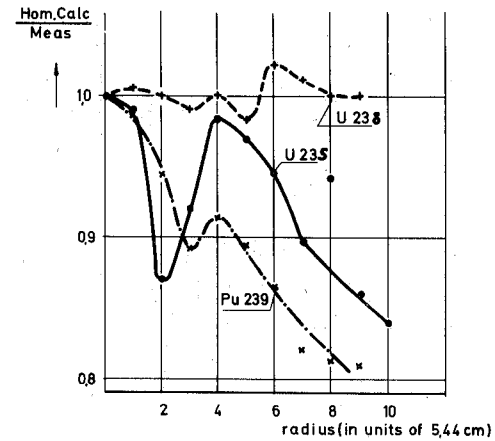
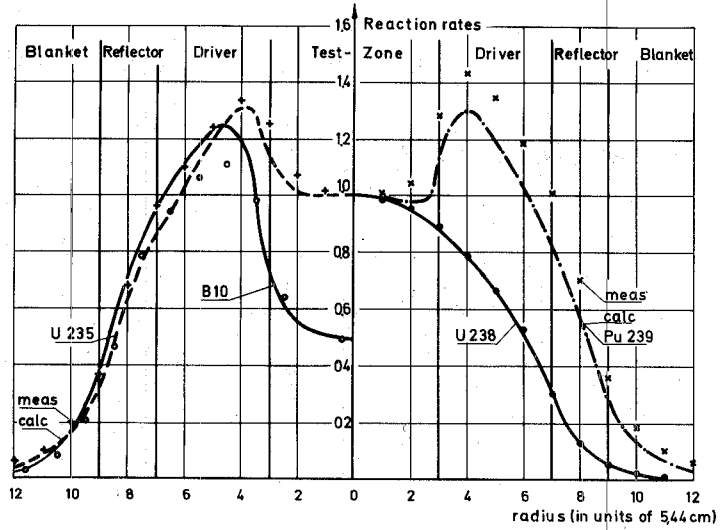


Fig.6 Rate Fine Structure within the Unit Cell, Driver Zone Pos. 16/20. \circ \times \bullet Exp.Points, Solid Line from ZERA Calc.



Homogeneous calculation



Heterogeneous calculation

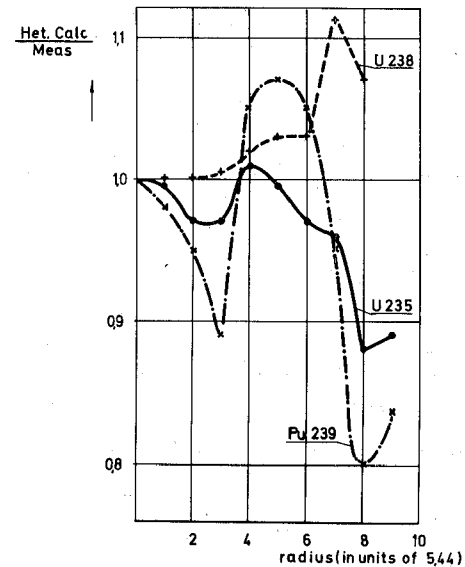
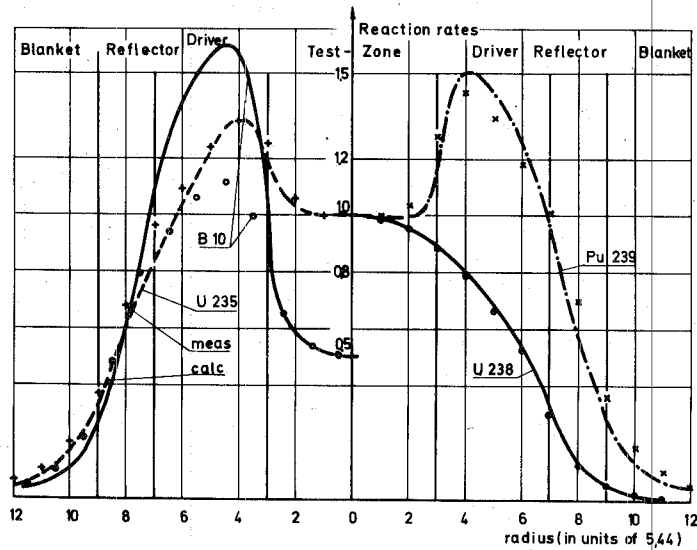
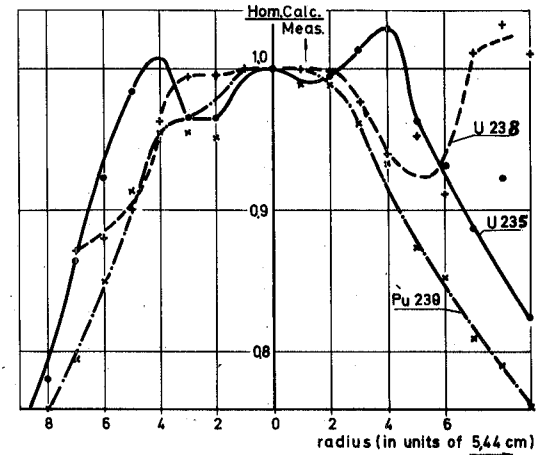
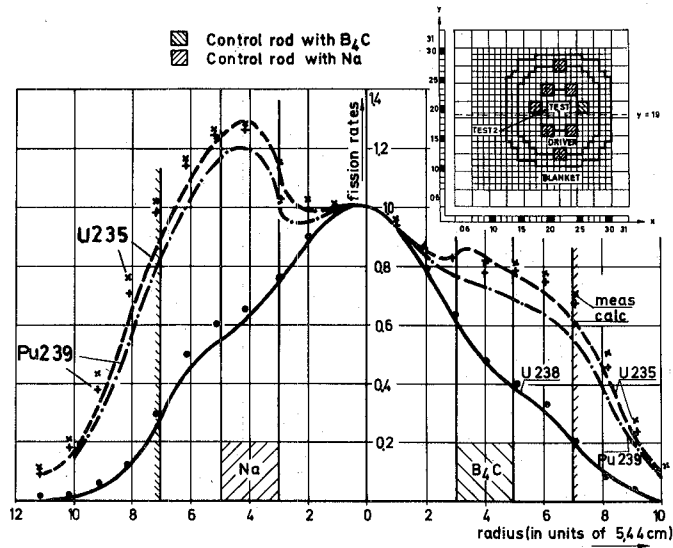


Fig.7 Radial Fission Chamber and B10 Traverses at Core Midplane, Y=19 in SNEAK-4 A

Radial Fission Chamber Traverses



Radial B10 Traverse

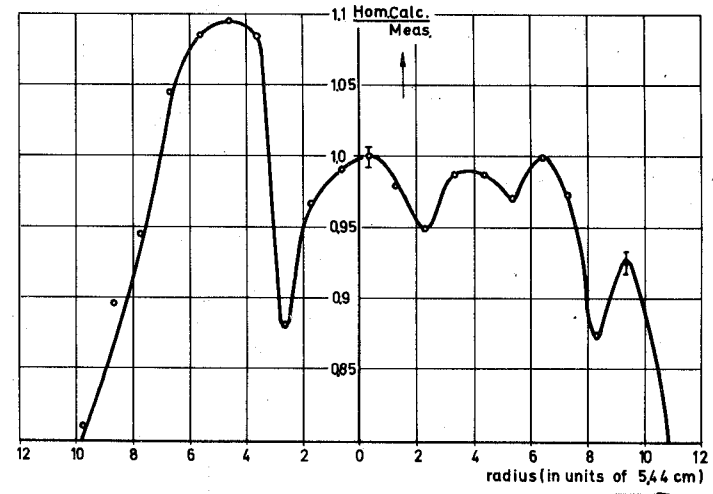
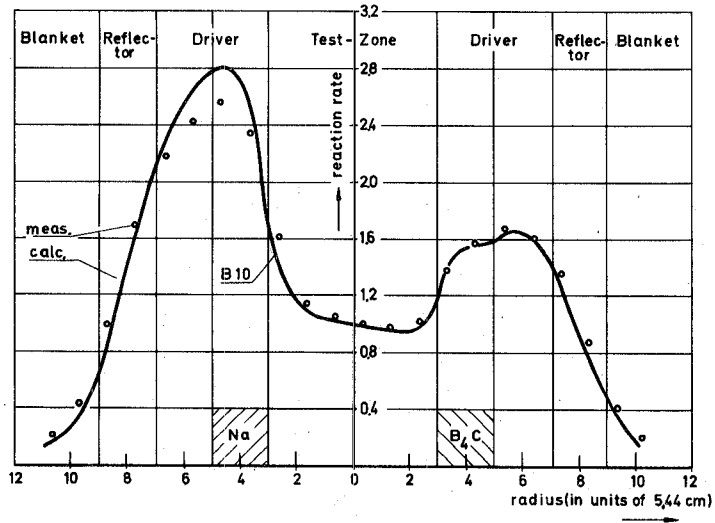


Fig.8 Radial Fission Chamber and B10 Traverses at Core Midplane, Y-19 in SNEAK-4B-11

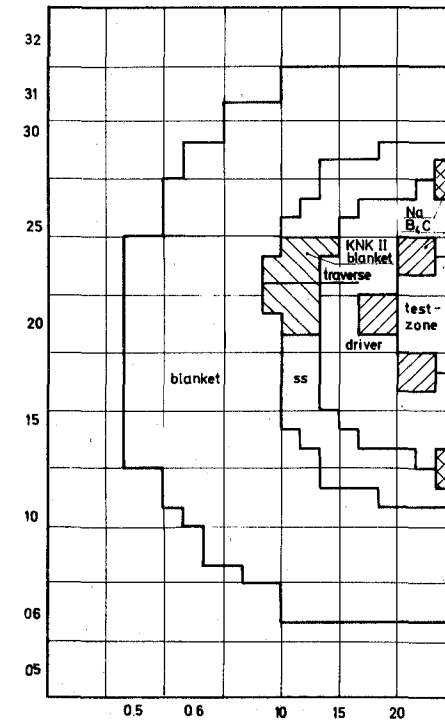
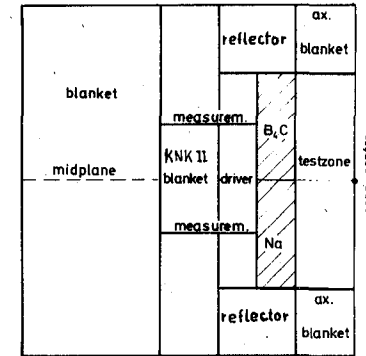
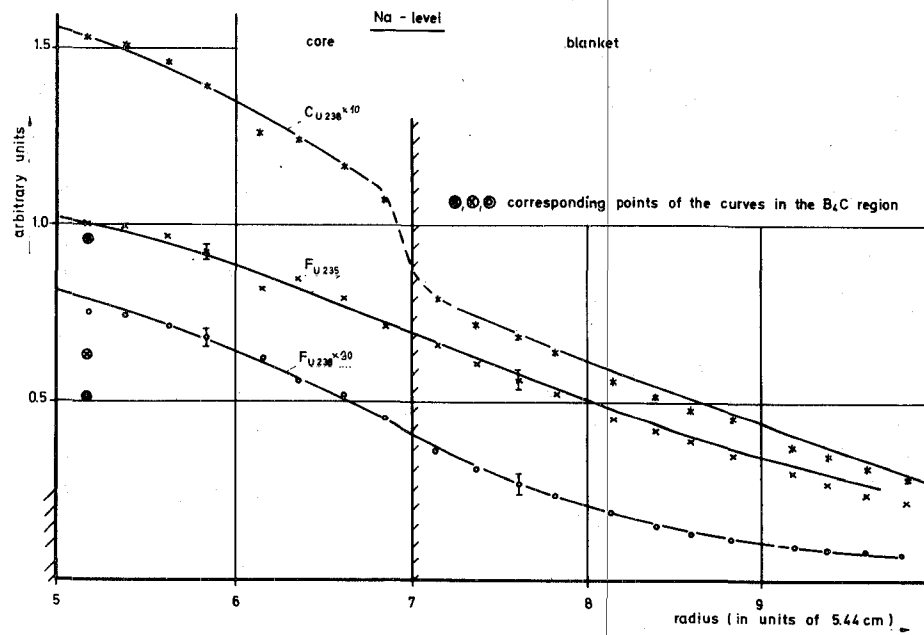
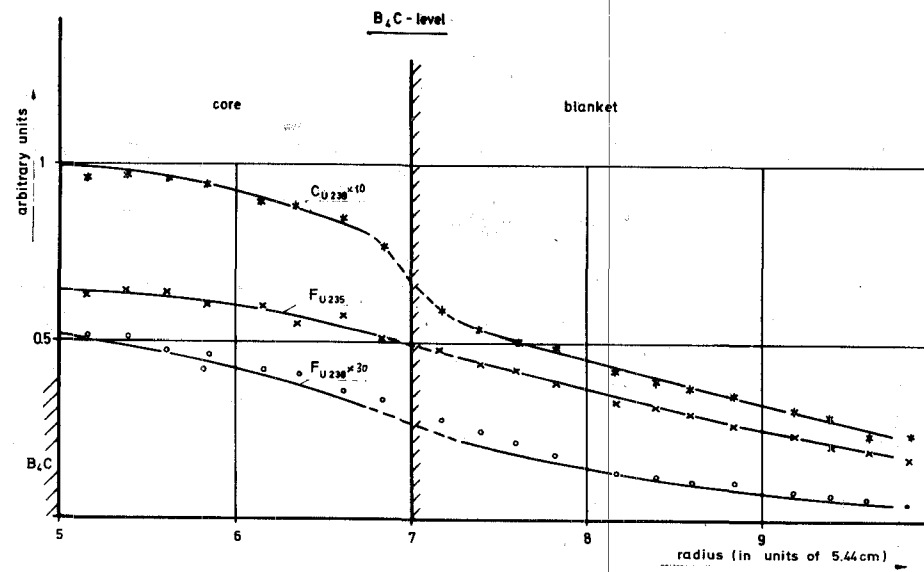


Fig.9 Comparison of Calculated and Experimental Reaction Rate Distribution in the outer Driver Region and in the Breeder Blanket, Foil Measurements

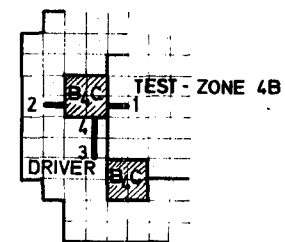
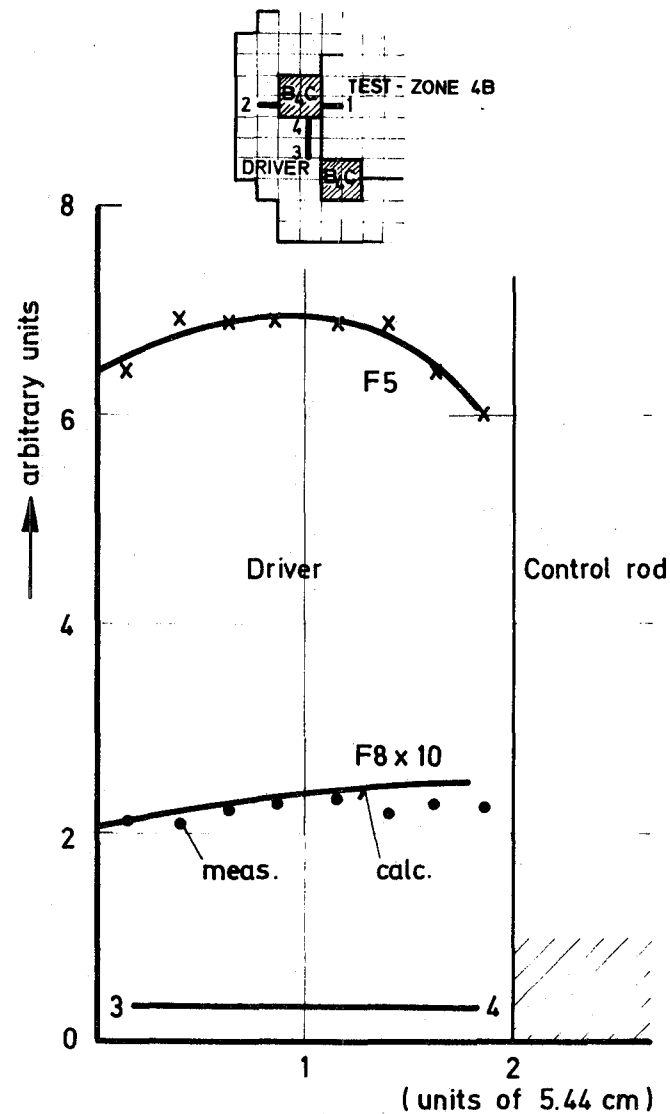
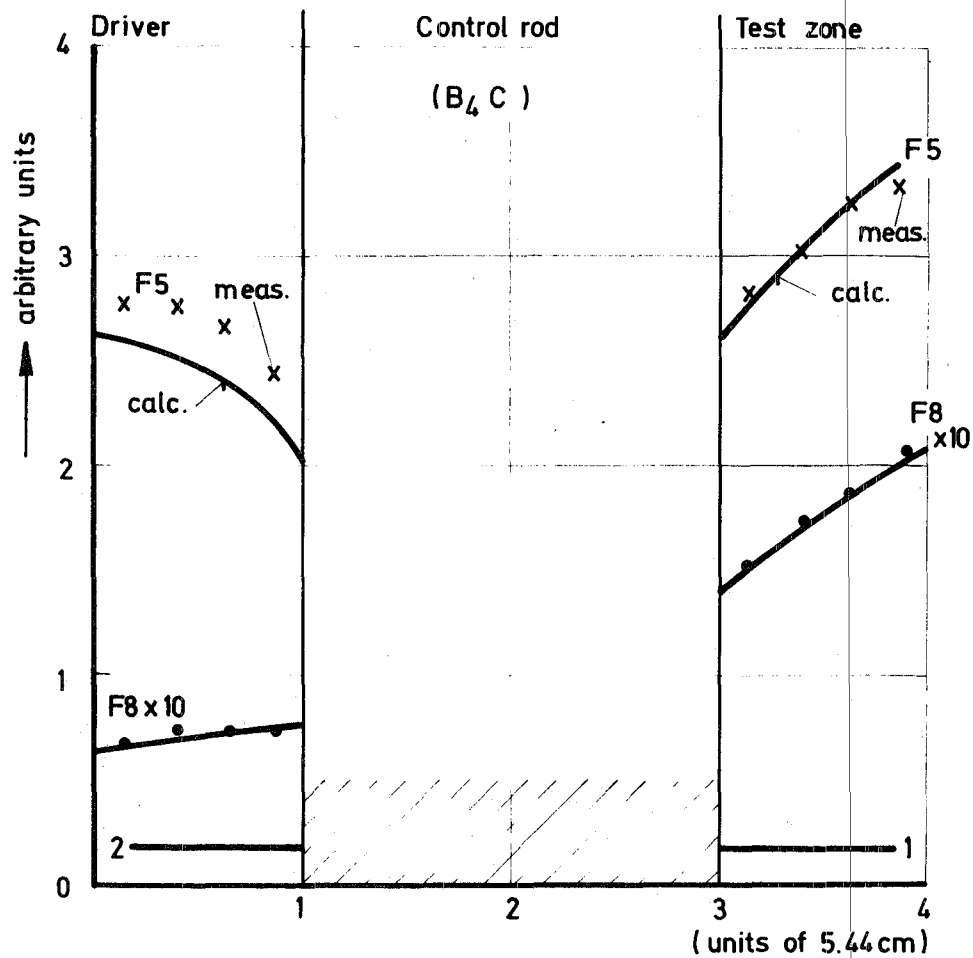


Fig.10 Rate Fine Traverses Near Absorber Rods (Foil Activation)

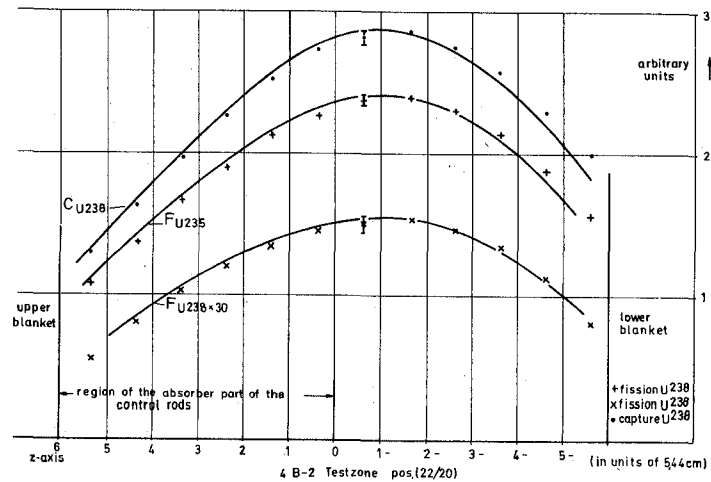
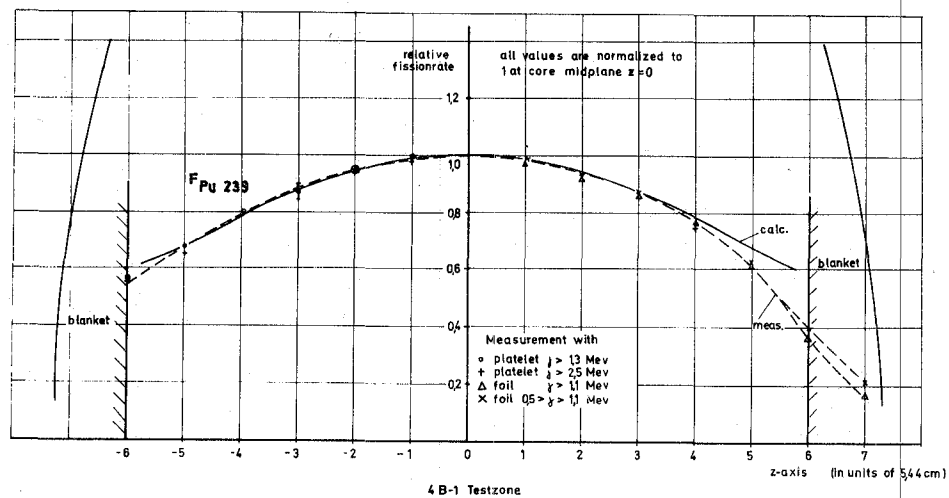
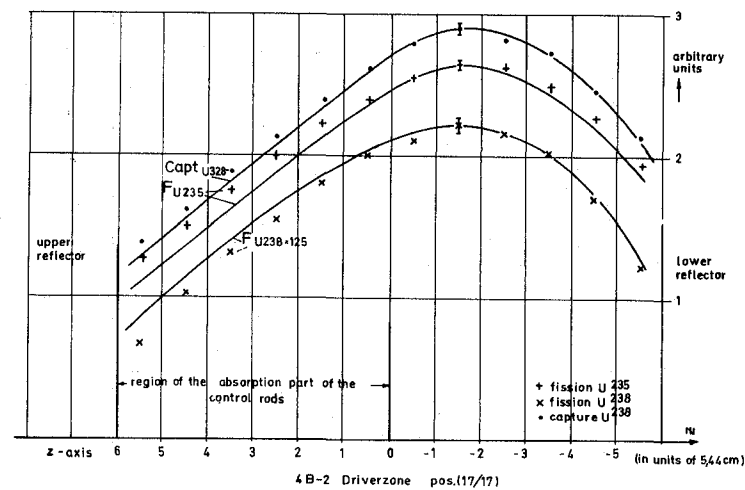
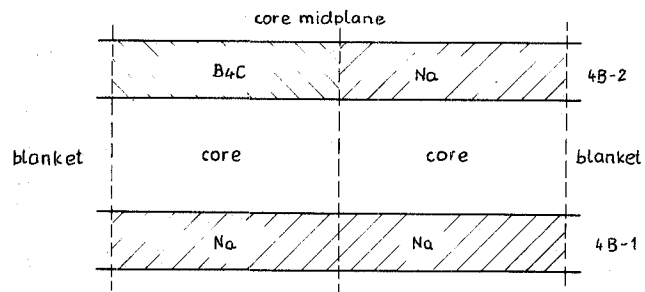


Fig. 11 Comparison of Calculated and Experimental Axial Reaction Rate Distributions in SNEAK-4B-1 and 4B-2 (Foil Activation)

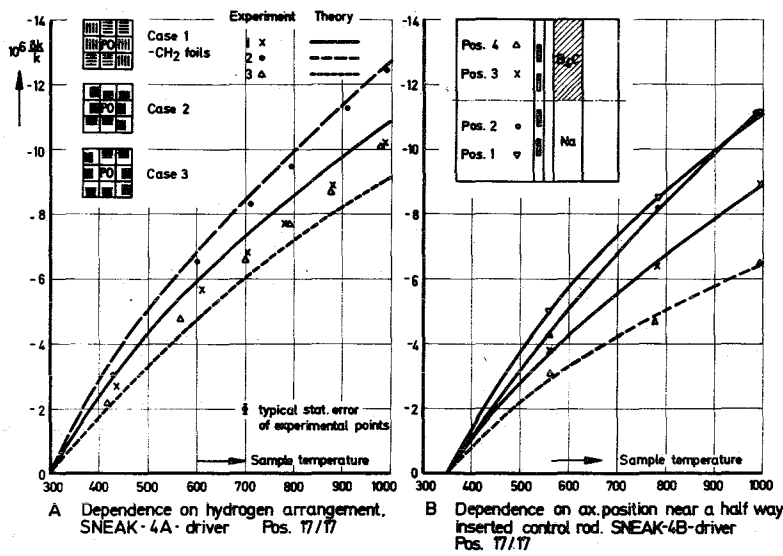
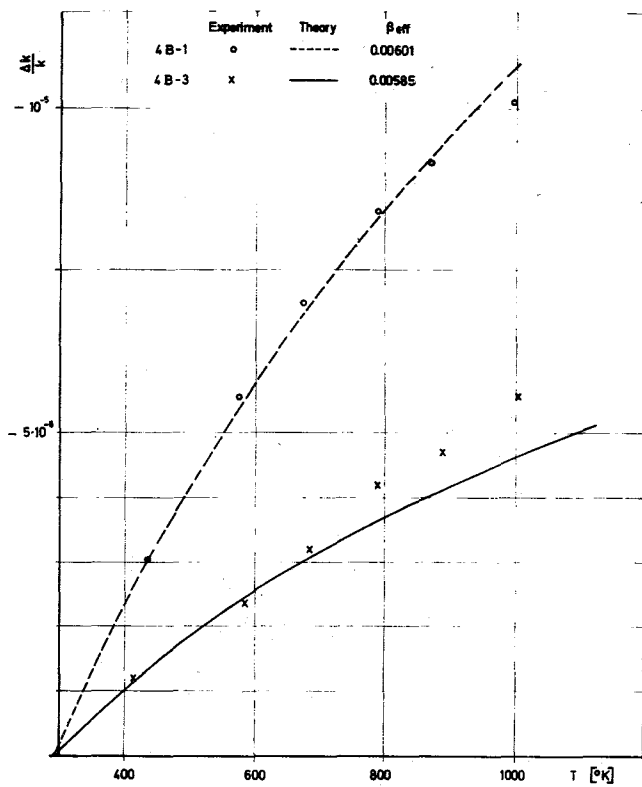
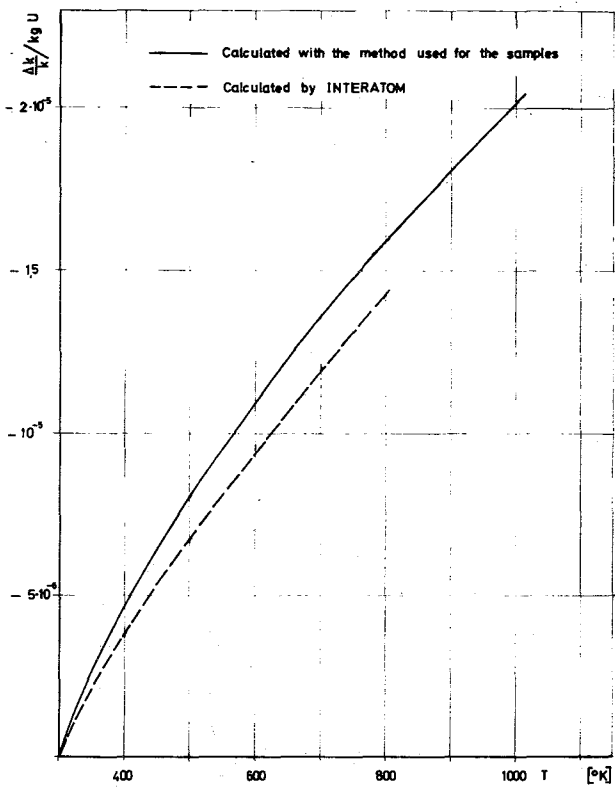


Fig.12 Doppler Effect Investigations

Top Left: Comparison of Calculational Techniques

Top Right: Doppler Measurements with a 25% Enriched UO_2 Sample in SNEAK 4B (Pos. 17/17)

Bottom: Study of Environmental Effects

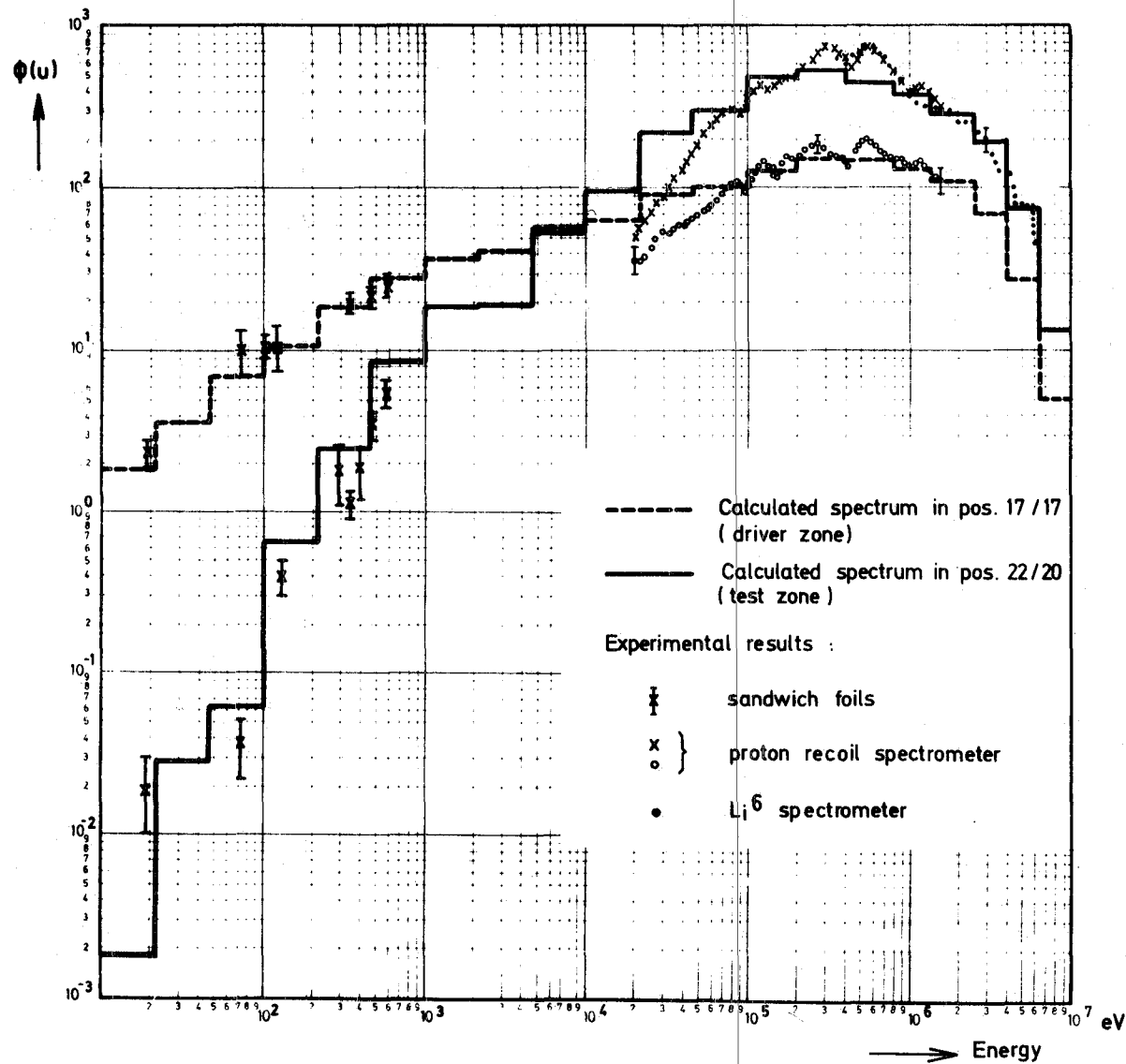
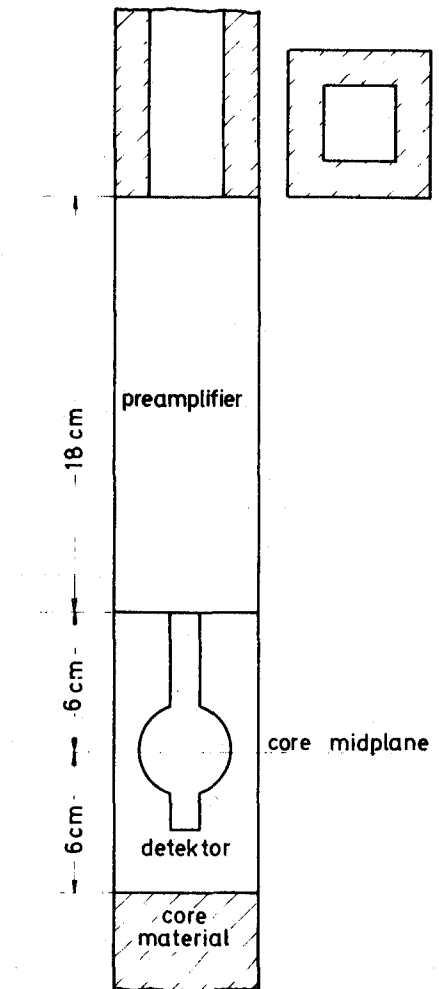


Fig.13 Neutron Spectra in Test and Driver Zone of SNEAK 4A



Proton Recoil Detector Arrangement

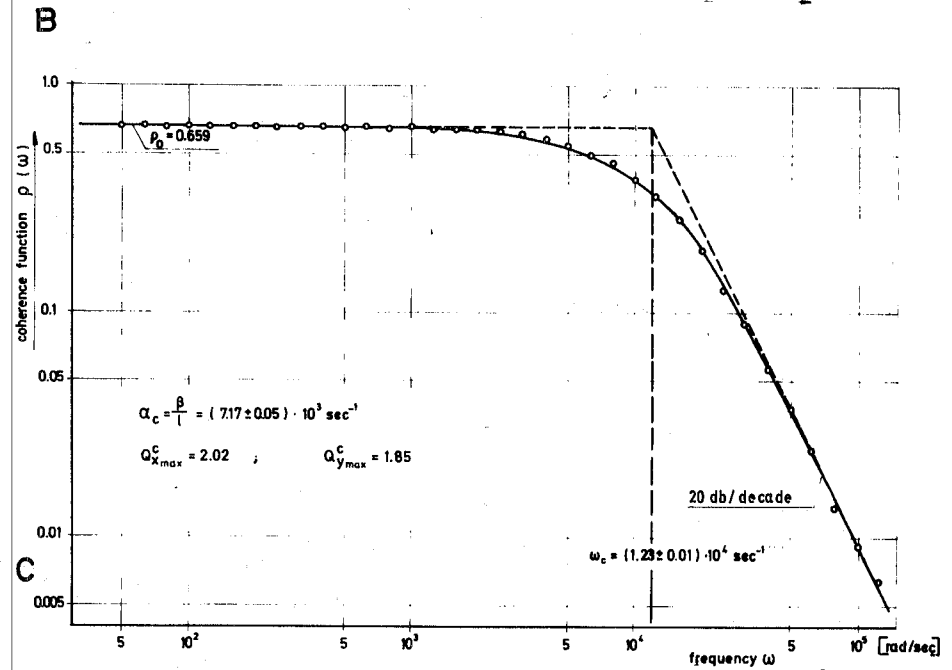
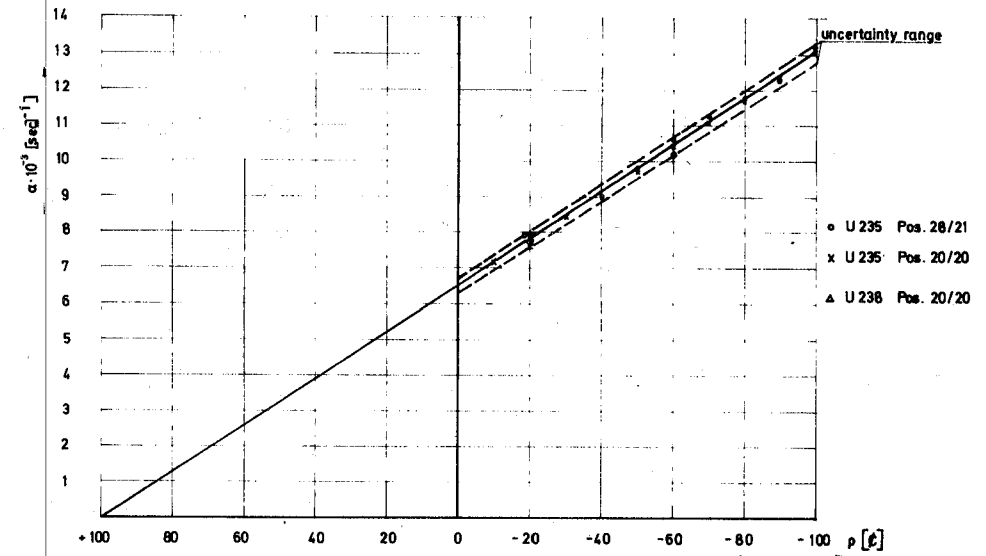
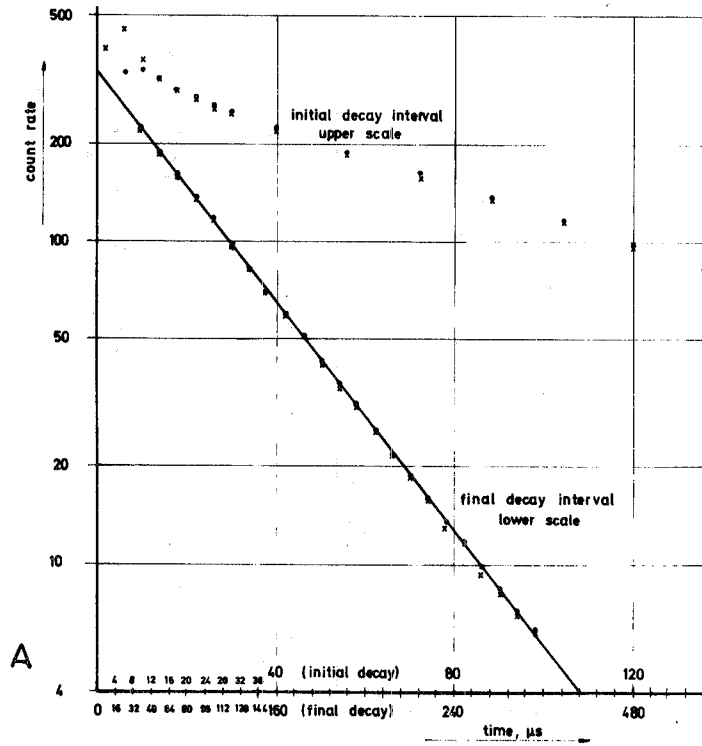


Fig. 14 A+B: Pulsed Source Measurements in SNEAK 4A

A: Prompt Neutron Decay at Core Center (x) and in the Reflector (o)

B: Prompt Neutron Decay Constant as a Function of Reactivity

C: Polarity Correlation Technique: Coherence Function for SNEAK-4 A

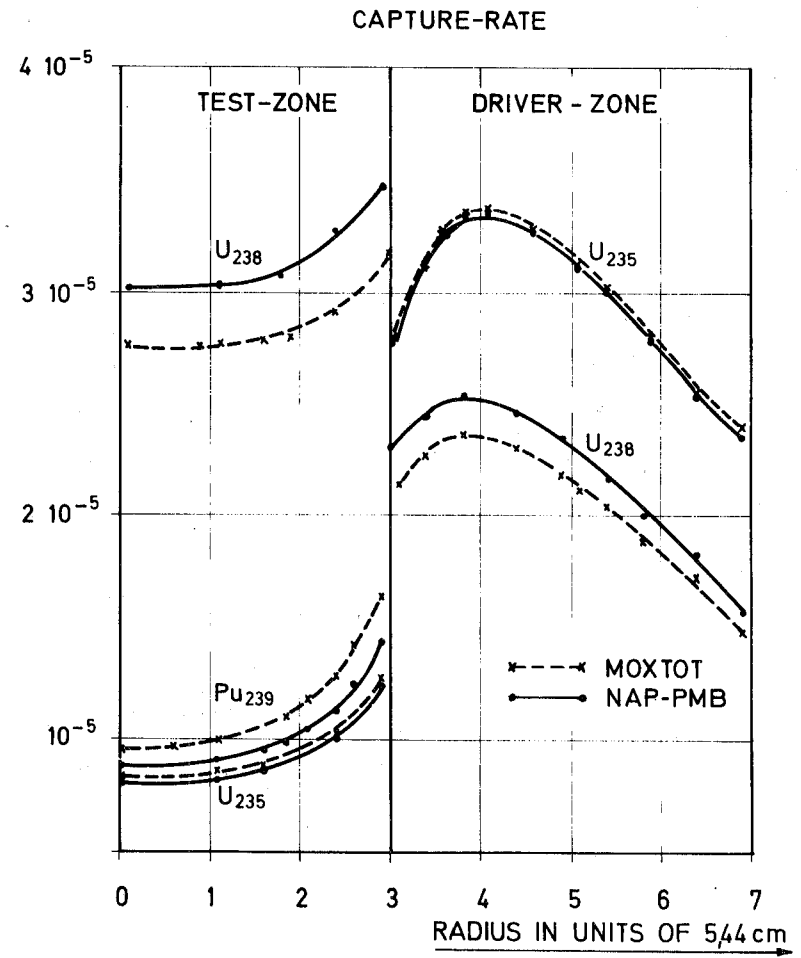
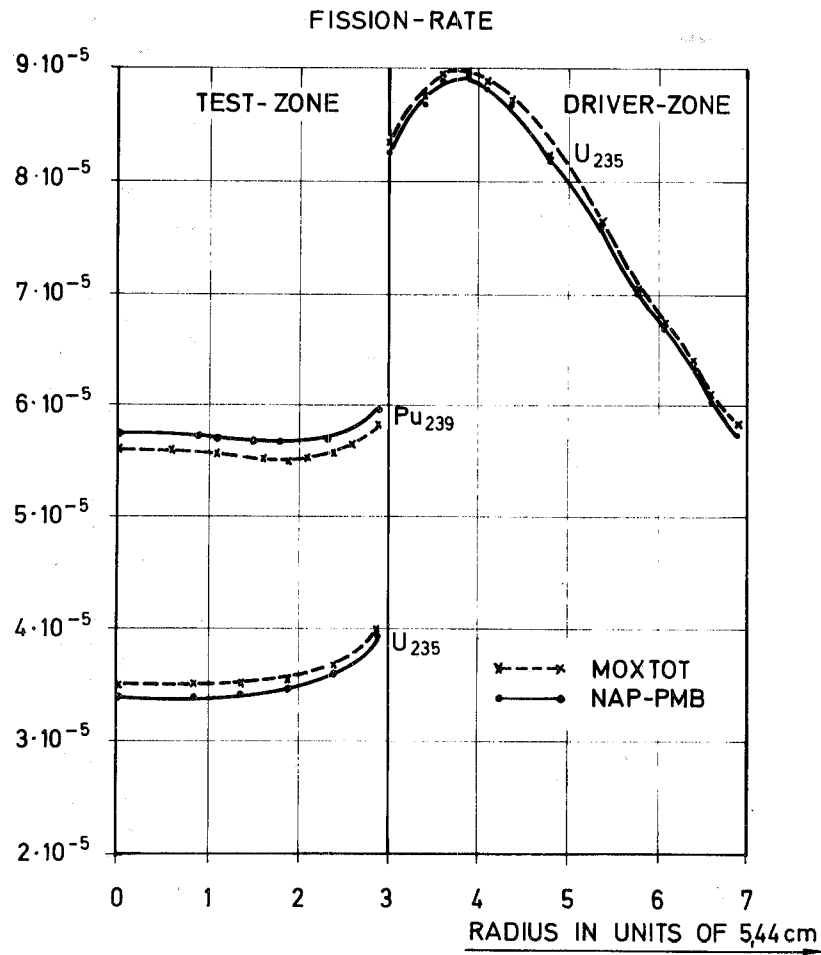


Fig.15 Comparison of Fission and Capture Rates in SNEAK 4 A Calculated with NAP-PMB and MOXTOT Set Respectively

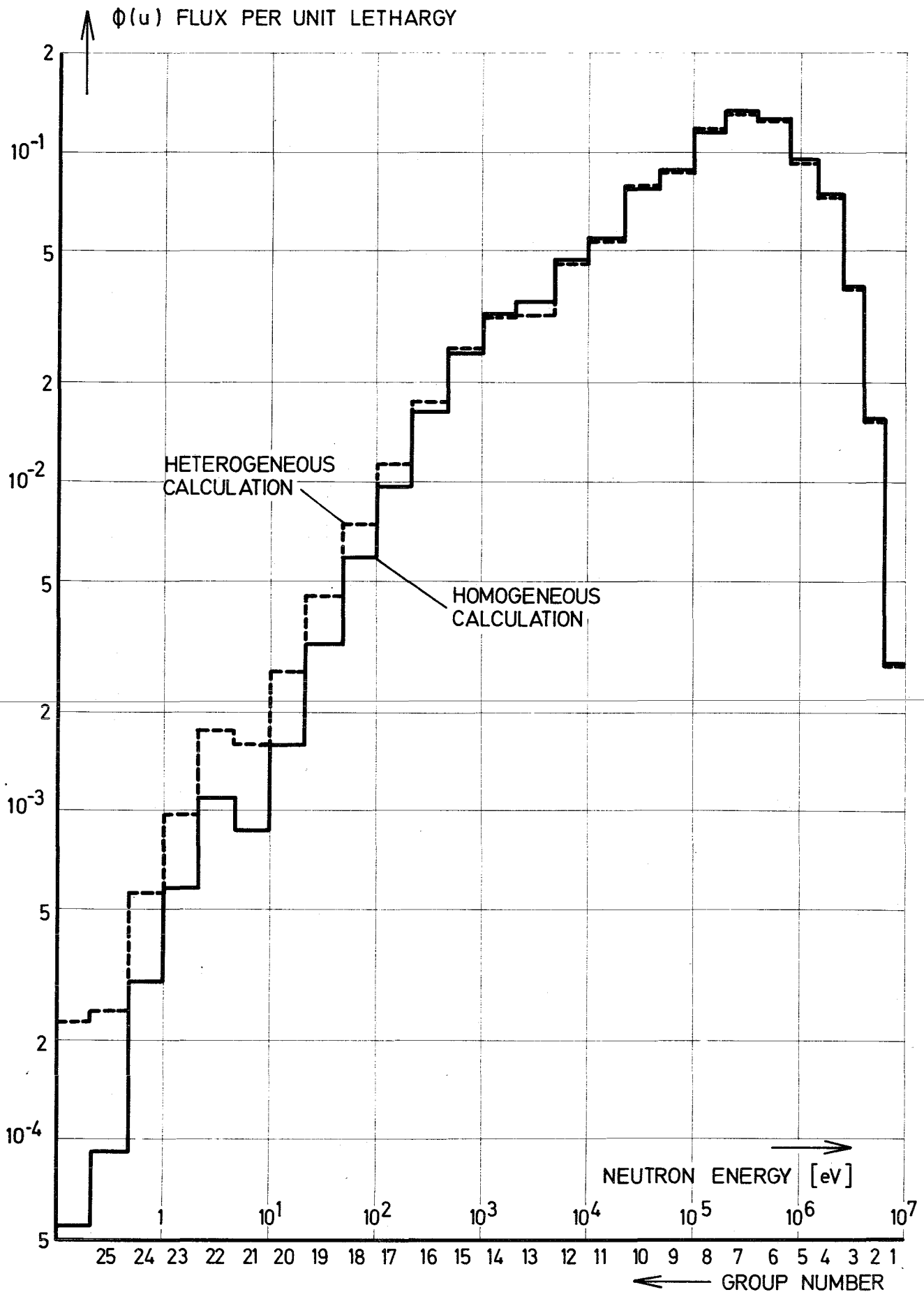


FIG. 16 NEUTRON SPECTRA IN THE DRIVER ZONE (R=30cm) CALCULATED WITH THE NAP PMB - SET